



1 **Global Soil Consumption of Atmospheric Carbon Monoxide:**
2 **An Analysis Using a Process-Based Biogeochemistry Model**

3 Licheng Liu¹, Qianlai Zhuang^{1,2}, Qing Zhu^{1,3}, Shaoqing Liu^{1,4}, Hella van Asperen⁵, Mari
4 Pihlatie^{6,7}

¹Department of Earth, Atmospheric, Planetary Sciences, Purdue University, West Lafayette, IN 47907,
USA

²Department of Agronomy, Purdue University, West Lafayette, IN 47907, USA

³Climate Sciences Department, Climate & Ecosystem Sciences Division, Lawrence Berkeley National
Laboratory, Berkeley, CA 94720, USA

⁴Department of Earth Sciences, University of Minnesota, Minneapolis, MN, 55455, USA

⁵Institute of Environmental Physics, University of Bremen, Otto-Hahn-Allee 1, Bremen, 28359, Germany

⁶Department of Physics, University of Helsinki, P.O. Box 48, 00014 University of Helsinki, Finland

⁷Department of Forest Sciences, P.O. Box 27, 00014 University of Helsinki, Finland

5 *Correspondence to:* Qianlai Zhuang(qzhuang@purdue.edu)

6

7



8 **Abstract:** Carbon monoxide (CO) plays an important role in controlling the
9 oxidizing capacity of the atmosphere by reacting with OH radicals that affect
10 atmospheric methane (CH₄) dynamics. We develop a process-based biogeochemistry
11 model to quantify CO exchange between the soil and the atmosphere at the global
12 scale. The model is parameterized using CO flux data from the field and laboratory
13 experiments for eleven representative ecosystem types. The model is then extrapolated
14 to the global terrestrial ecosystems. Global soil gross consumption, gross production,
15 and net flux of the atmospheric CO are estimated to be 132-154, 29-36 and 102-119 Tg
16 CO yr⁻¹ (1Tg = 10¹² g), respectively, assuming a constant spatially distributed
17 atmospheric CO concentration (~128 ppbv) during the 20th century. When satellite-
18 based atmospheric CO concentration data are used, our estimates of the soil gross
19 consumption are 180-197 Tg CO yr⁻¹ in the period of 2000-2013. Tropical evergreen
20 forest, savanna and deciduous forest areas are the largest sinks at 93 Tg CO yr⁻¹. Soil
21 CO gross consumption is sensitive to air temperature and atmospheric CO
22 concentration while gross production is sensitive to soil organic carbon (SOC) stock and
23 air temperature. Under future climate scenarios, the soil gross consumption, gross
24 production and net flux of CO will increase at 0.15-1.23, 0.04-0.3 and 0.12-0.94 Tg CO
25 yr⁻² during 2014-2100, reaching 162-194, 36-44, and 126-150 Tg CO yr⁻¹ by the end of
26 the 21st century, respectively. Areas near the equator, Eastern US, Europe and eastern
27 Asia will be the largest sinks due to optimum soil moisture and high temperature. The
28 annual global soil net flux of atmospheric CO is primarily controlled by air temperature,
29 soil temperature, SOC and atmospheric CO concentrations, while its monthly variation
30 mainly determined by air temperature, precipitation, soil temperature and soil moisture.
31 Our process-based soil CO dynamics model and analysis shall benefit the modeling of
32 the global climate and atmospheric chemistry.

33

34 1. Introduction

35 Carbon monoxide (CO) plays an important role in controlling the oxidizing
36 capacity of the atmosphere by reacting with OH radicals (Logan et al., 1981; Crutzen,
37 1987; Khalil & Rasmussen, 1990; Prather et al., 1995; Prather & Ehhalt, 2001). CO in
38 the atmosphere can directly and indirectly influence the fate of critical greenhouse



39 gases such as methane (CH₄) and ozone (O₃) (Logan et al., 1981; Crutzen & Gidel,
40 1983; Guthrie, 1989; Khalil & Rasmussen, 1990; Lu & Khalil, 1993; Daniel & Solomon,
41 1998; Prather & Ehhalt, 2001; Tan and Zhuang, 2012). Although CO itself absorbs only
42 a limited amount of infrared radiation from the Earth, the cumulative indirect radiative
43 forcing of CO may be even larger than that of the third powerful greenhouse gas, nitrous
44 oxide (N₂O, Myhre et al., 2013). Current estimates of global CO emissions from both
45 anthropogenic and natural sources range from 1550 to 2900 Tg CO yr⁻¹, which are
46 mainly from anthropogenic and natural direct emissions and from the oxidation of
47 methane and other Volatile Organic Compounds (VOC) (Prather et al., 1995; Khalil et
48 al., 1999; Bergamaschi et al., 2000; Prather & Ehhalt, 2001, Stein et al., 2014).
49 Chemical consumption of CO by atmospheric OH and the biological consumption of CO
50 by soil microbes are two major sinks of the atmospheric CO (Conrad, 1988; Lu & Khalil,
51 1993; Prather et al., 1995; Prather & Ehhalt, 2001; Yonemura et al., 2000; Whalen &
52 Reeburgh, 2001).

53 Soils are globally considered as a major sink for CO due to microbial activities
54 (Conrad and Seiler, 1982; Potter et al., 1996; Whalen and Reeburgh, 2001; King and
55 Weber, 2007). A diverse group of soil microbes including carboxydrotrophs,
56 methanotrophs and nitrifiers are capable of oxidizing CO (Ferenci et al., 1975; Jones
57 and Morita, 1983; Bender and Conrad, 1994; King and Weber, 2007). Annually, 10-25%
58 of CO emissions were consumed by soils (Sanhueza et al., 1998; Khalil et al., 1999;
59 King, 1999a; Bergamaschi et al., 2000; Prather & Ehhalt, 2001; Chan & Steudler, 2006).
60 Potter et al. (1996) reported the global soil consumption be 16-50 Tg CO yr⁻¹, by using a
61 single box model approach over the upper 5 cm of soils. Other estimates showed large
62 ranges using simple assumptions, such as 115–230 Tg CO yr⁻¹ based on a constant
63 dry deposition velocity (the uptake rate divided by the CO concentration) of 0.03 cm s⁻¹
64 (Sanhueza et al., 1998); 300 Tg CO yr⁻¹ using the same constant deposition velocity
65 and zero deposition velocity value in deserts and areas with monthly mean
66 temperatures below 0 °C with different approaches (Bergamaschi et al., 2000); 190-580
67 Tg CO yr⁻¹ using empirical approaches with a higher probability for lower values (King,
68 1999). Besides, reported CO dry deposition velocities (0 to 0.004m s⁻¹) for vegetated
69 surfaces based on measurements are relatively low compared with other substances



70 (King, 1999a; Castellanos et al., 2011). To date, there are still large uncertainties in
71 estimating soil CO consumption, ranging from 15 to 640 Tg CO yr⁻¹. Although soil CO
72 consumption and its environmental controls have been heavily studied, the impacts of
73 long-term changes in climate and human activities on the atmosphere-biosphere CO
74 exchange are still not clear (King & Weber, 2007; Vreman et al., 2011; He and He, 2014;
75 Pihlatie et al., 2016). Moreover, production of CO has been widely found in soils, plant
76 roots, living and degrading plant materials and degrading organic matter (Pihlatie et al.,
77 2016). CO production is dominantly due to abiotic processes such as thermal- and
78 photo-degradation of organic matter or plant material (Conrad and Seiler, 1985b; Tarr et
79 al., 1995; Schade et al., 1999; Derendorp et al., 2011; Lee et al., 2012; van Asperen et
80 al., 2015; Fraser et al., 2015, Pihlatie et al., 2016), except for a few cases of anaerobic
81 formations. Photo-degradation includes direct photo-degradation due to absorbing
82 radiation by light-absorbing molecules and indirect photo-degradation due to radiation
83 energy transferring to non-light-absorbing molecules (King et al., 2012). Thermal-
84 degradation is identified as the temperature-dependent degradation of carbon in the
85 absence of radiation and possibly oxygen (Derendorp et al., 2011; Lee et al., 2012; van
86 Asperen et al., 2015; Pihlatie et al., 2016). Previous field and laboratory studies on the
87 role of direct or indirect abiotic degradation showed very contrasting results, primarily
88 due to the challenge of separation between CO formation through thermal-degradation
89 and photo-degradation, because they can both occur simultaneously and the indirect
90 photo-degradation may occur even without solar radiation if thermal energy is suitable
91 (Lee et al., 2012).

92 Little focus has been placed so far on the role of net CO budget (including soil
93 CO consumption and production) in global climate modeling. Most top-down models
94 apply a dry deposition scheme based on the resistance model of Wesely (1989). Such
95 schemes give a wide range of dry deposition velocities (Stevenson et al., 2006). Only a
96 few models (MOZART-4, Emmons et al., 2010; CAM-chem, Lamarque et al., 2012)
97 have extended their dry deposition schemes with a parameterization for CO and H₂
98 uptake by oxidation from soil bacteria and microbes following the work of Sanderson et
99 al. (2003), which itself was based on extensive measurements from Yonemura et al.
100 (2000). Potter et al. (1996) developed a bottom-up model to simulate CO consumption



101 and production at the global scale. This model is a single box model, only considers top
102 5cm depth of soil and does not have explicit microbial factors, which might have
103 underestimated CO consumption (Potter et al., 1996; King, 1999a). Current bottom-up
104 CO modeling approaches are mostly based on a limited number of CO *in situ*
105 observations or laboratory studies to quantify regional and global soil consumption
106 (Potter et al., 1996; Sanhueza et al., 1998; Khalil et al., 1999; King, 1999a;
107 Bergamaschi et al., 2000; Prather & Ehhalt, 2001). To our knowledge, no detailed
108 process-based model of soil-atmospheric exchange of CO has been published in the
109 recent 15 years. One reason is an incomplete understanding of biological processes of
110 CO emission and uptake (King & Weber, 2007; Vreman et al., 2011; He and He, 2014;
111 Pihlatie et al., 2016). Another reason is a lack of long-term CO flux measurements for
112 different ecosystem types to calibrate and evaluate the models. CO flux measurements
113 are mostly from short-term field observations or laboratory experiments (e.g. Conrad
114 and Seiler, 1985a; Funk et al., 1994; Tarr et al., 1995; Zepp et al., 1997; Kuhlbusch et
115 al., 1998; Moxley and Smith, 1998; Schade et al., 1999; King and Crosby, 2002; Varella
116 et al., 2004; Lee et al., 2012; Bruhn et al., 2013; van Asperen et al., 2015). The first
117 study to report long-term and continuous field measurements of CO flux over grassland
118 using a micrometeorological eddy covariance (EC) method are in Pihlatie et al. (2016).

119 Aiming to improve the understanding of processes associated with land-
120 atmosphere CO exchange and to quantify global soil CO budget for the 20th and 21st
121 centuries, we developed a CO dynamics module (CODM) embedded in a process-
122 based biogeochemistry model, the Terrestrial Ecosystem Model (TEM) (Zhuang et al.,
123 2003, 2004, 2007). CODM was then calibrated and evaluated using laboratory
124 experiments and field measurements for different ecosystem types. We then used the
125 atmospheric CO concentration data from MOPITT (Gille, 2013) to drive our model from
126 2000 to 2013. We conducted century-long simulations of 1901-2100, using the
127 atmospheric CO concentrations estimated with an empirical function (Badr & Probert,
128 1994; Potter et al., 1996). We also evaluated the effects of multiple forcings on global
129 CO consumption and production estimates, including the changes of climate and
130 atmospheric CO concentrations at the global scale.

131



132 2. Method

133 2.1 Overview

134 We first developed a daily soil CO dynamics module (CODM) that considers: (1)
135 soil-atmosphere CO exchange and diffusion process between soil layers, (2)
136 consumption by soil microbial oxidation, (3) production by soil chemical oxidation, and
137 (4) the effects of temperature, soil moisture, soil CO substrate and surface atmospheric
138 CO concentration on these processes. Second, we used observed soil temperature and
139 moisture to evaluate TEM hydrology module and soil thermal module in order to
140 estimate soil physical variables correctly. Then we used results of laboratory
141 experiments and CO flux measurements to parameterize the model and calibrate the
142 model using the Shuffled Complex Evolution (SCE-UA) method (Duan et al., 1993).
143 Finally, the model was extrapolated to the global scale at a 0.5° by 0.5° resolution. We
144 conducted three sets of model experiments to investigate the impact of climate and
145 atmospheric CO concentrations on soil CO dynamics: 1) 1901-2013 with constant
146 atmospheric CO concentrations estimated from an empirical function; 2) 2000-2013 with
147 MOPITT satellite atmospheric CO concentration data; and 3) 2014-2100 with the same
148 constant atmospheric CO concentrations as 1) and three future climate scenarios.

149

150 2.2 Carbon Monoxide Dynamics Module (CODM)

151 Embedded in TEM (Figure 1), CODM is mainly driven by: (1) soil organic carbon
152 availability based on a carbon and nitrogen dynamics module (CNDM) (Zhuang et al.,
153 2003); (2) soil temperature profile from a soil thermal module (STM) (Zhuang et al.,
154 2001, 2003); and (3) soil moisture profile from a hydrological module (HM) (Bonan,
155 1996; Zhuang et al, 2004). Net exchange of CO between the atmosphere and soil is
156 determined by the mass balance. According to previous studies, we separate active
157 soils (top 30cm) for CO consumption and production into 1 cm thick layers (King, 1999a,
158 1999b; Whalen & Reeburgh, 2001; Chan & Steudler, 2006). Between the soil layers, the
159 changes of CO concentrations are calculated by:

$$\frac{\partial(C(t, i))}{\partial t} = \frac{\partial}{\partial z} \left(D(t, i) \frac{\partial(C(t, i))}{\partial z} \right) + P(t, i) - O(t, i) \quad (1)$$



160 Where $C(t, i)$ is the CO concentration in layer i and time t , units are mg m^{-3} . z is the
 161 thickness of layer i . $D(t, i)$ is the diffusion coefficient for layer i , units are $\text{m}^2 \text{s}^{-1}$. $P(t, i)$
 162 is the CO production rate and $O(t, i)$ is CO consumption rate due to oxidation. The units
 163 of $P(t, i)$ and $O(t, i)$ are $\text{mg m}^{-3} \text{s}^{-1}$. $D(t, i)$ is calculated using the method from Potter et
 164 al. (1996), equation (2) to (4), which is the function of soil temperature, soil texture and
 165 soil moisture. The upper boundary condition is specified as the atmospheric CO
 166 concentration, which is estimated by an empirical function of latitude (Potter et al., 1996)
 167 or directly measured by the MOPITT satellite during 2000-2013. The lower boundary
 168 condition is assumed to have no diffusion exchange with the layer underneath. This
 169 partial differential equation (PDE) is solved using the Crank-Nicolson method for less
 170 time-step-sensitive solution.

171 CO consumption is modeled as an aerobic process occurring in unsaturated soil
 172 pores, which is estimated as:

$$O(t, i) = V_{max} \cdot f_1(C(t, i)) \cdot f_2(T(t, i)) \cdot f_3(M(t, i)) \quad (2)$$

173 Where V_{max} is the specific maximum oxidation rate, ranging from 0.3 to 11.1 $\mu\text{g CO g}^{-1}$
 174 h^{-1} (Whalen & Reeburgh, 2001). f_i are functions calculating CO concentration $C(t, i)$,
 175 temperature $T(t, i)$ and moisture $M(t, i)$ influences on CO soil consumption.
 176 Considering CO consumption as the result of microbial activities, we calculate
 177 $f_1(C(t, i))$, $f_2(T(t, i))$ and $f_3(M(t, i))$ in a similar way as Zhuang et al. (2004):

$$f_1(C(t, i)) = \frac{C(t, i)}{C(t, i) + k_{CO}} \quad (2.1)$$

$$f_2(T(t, i)) = Q_{10}^{\frac{T(t, i) - T_{ref}}{10}} \quad (2.2)$$

$$f_3(M(t, i)) = \frac{(M(t, i) - M_{min})(M(t, i) - M_{max})}{(M(t, i) - M_{min})(M(t, i) - M_{max}) - (M(t, i) - M_{opt})^2} \quad (2.3)$$

178 Where $f_1(C(t, i))$ is a multiplier that enhances oxidation rate with increasing soil CO
 179 concentrations using a Michaelis-Menten function with a half-saturation constant k_{CO} ,
 180 ranging from 5 to 51 $\mu\text{l CO l}^{-1}$ (Whalen & Reeburgh, 2001); $f_2(T(t, i))$ is a multiplier that
 181 enhances CO oxidation rates with increasing soil temperature using a Q10 function with
 182 Q_{10} coefficients (Whalen & Reeburgh, 2001). T_{ref} is the reference temperature, units



183 are °C (Zhuang et al., 2004, 2013). $f_3(M(t, i))$ is a multiplier to estimate the biological
 184 limiting effect that diminishes CO oxidation rates if the soil moisture is not at an optimum
 185 level (M_{opt}). M_{min} , M_{max} and M_{opt} are the minimum, maximum and optimum volumetric
 186 soil moistures of oxidation reaction, respectively. Equation (2.2) will overestimate CO
 187 consumption at higher temperature because CO consumption has an optimum
 188 temperature and it will decrease at higher temperatures. However, the CO consumption
 189 is constrained by CO production, and equation (1) is used to represent this constraint.

190 We model the CO production rate ($P(t, i)$) as a process of chemical oxidation
 191 constrained by soil organic carbon (SOC) decay (Conrad and Seiler, 1985; Potter et al.
 192 1996; Jobbagy & Jackson, 2000; van Asperen et al., 2015):

$$P(t, i) = P_r(t, i) \cdot E_{SOC} \cdot C_{SOC}(t) \cdot F_{SOC} \quad (3)$$

193 Where $P_r(t, i)$ is a reference soil CO production rate which has been normalized to rate
 194 at reference temperature, which is affected by soil moisture and soil temperature
 195 (Conrad and Seiler, 1985; van Asperen et al., 2015). E_{SOC} is an estimated nominal CO
 196 production factor of $3.5 \pm 0.9 \times 10^{-9}$ mg CO m⁻² s⁻¹ per g SOC m⁻² (to 30 cm surface soil
 197 depth) (Potter et al., 1996). $C_{SOC}(t)$ is a SOC content in mg m⁻², which is provided by
 198 CNDM module in TEM. F_{SOC} is a constant fraction of top 20cm SOC compared to total
 199 amount of SOC, which is 0.33 for shrubland areas, 0.42 for grassland areas and 0.50
 200 for forest areas, respectively (Jobbagy & Jackson, 2000). $P_r(t, i)$ is calculated as:

$$P_r(t, i) = \exp\left(f_4(M(t, i)) \cdot Ea_{ref}/R \cdot \left(\frac{1}{273.15 + PT_{ref}} - \frac{1}{T(t, i) + 273.15}\right)\right) \quad (3.1)$$

$$f_4(M(t, i)) = \frac{PM_{ref}}{M(t, i) + PM_{ref}} \quad (3.2)$$

201 Where equation (3.1) is derived from Arrhenius equation for chemical reactions and
 202 normalized using the reference temperature PT_{ref} . Ea_{ref}/R is the reference activation
 203 energy divided by gas constant R , units are K. $f_4(M(t, i))$ is the multiplier that reduces
 204 activation energy using an regression approach based on laboratory experiment of
 205 moisture influences on CO production (Conrad and Seiler, 1985). PM_{ref} is the reference
 206 volumetric soil moisture, ranging from 0.01 to 0.5 volume/volume (v/v). We assume



207 thermal-degradation as the main CO producing process since lack of photo-degradation
208 data and hard to distinguish photo-degradation from observations. In order to reduce
209 the bias from thermal-degradation to total abiotic degradation, the equation (3.1) is
210 parameterized by comparing with total production rate. For instance, $P_r(t, i)$ calculation
211 can perfectly fit the experiment results in Van Asperen et al., 2015 with proper
212 $PT_{ref}(18^\circ\text{C})$, $Ea_{ref}/R(14000\text{ K})$ and $PM_{ref}(0.5\text{ v/v})$.

213

214 **2.3 Model Parameterization and Extrapolation**

215 The model parameterization was conducted in two steps: 1) Thermal and
216 hydrology modules embedded in TEM were revised, calibrated and evaluated by
217 running model with corresponding local meteorological or climatic data at 4
218 representative sites, including boreal forest, temperate forest, tropical forest and
219 savanna (Table 1, site No.1 to 4, Figure 2) to minimize model data misfit in terms of soil
220 temperature and moisture. 2) CODM module was parameterized by running TEM for
221 observational periods with the corresponding local meteorological or climatic data at
222 each reference site (Table 1, Figure 3), and using Shuffled Complex Evolution
223 Approach in R language (SCE-UA-R) (Duan et al., 1993) to minimize the difference
224 between simulated and observed net CO flux. Eleven parameters including k_{CO} , V_{max} ,
225 T_{ref} , Q_{10} , M_{min} , M_{max} , M_{opt} , E_{SOC} , Ea_{ref}/R , PM_{ref} and PT_{ref} are optimized (Table 2). To
226 be noticed, F_{SOC} was not involved in the calibration process. Parameter priors were
227 decided based on previous studies (Conrad & Seiler, 1985; King, 1999b; Whalen &
228 Reeburgh, 2001; Zhuang et al., 2004). SCE-UA-R was used for site No. 6, 8, 10, 11
229 (Table 1). Each site had been run 50 times using SCE-UA-R with 10000 maximum
230 loops for parameter ensemble, and all of them reached stable state before the end of
231 the loops. For wetlands, the only available data is from site No.12. We used trial-and-
232 error method instead to make our simulated results in the range of observed flux rates,
233 with a 10% tolerance. For tropical sites, since tropical savanna vegetation type is a
234 combination type of tropical forest and grassland in our model, we first used Site No. 13
235 to set priors to fit the experiment results with a 10% tolerance and then evaluated by
236 running our model comparing with site No.7 results. Site No. 9 and 5 were used to
237 evaluate our model results for temperate forest and grassland. Besides the observed



238 climatic and soil property data, we used ERA-Interim reanalysis data from The
239 European Centre for Medium-Range Weather Forecasts (ECMWF) (Dee et al., 2011),
240 AmeriFlux observed meteorology data (<http://ameriflux.lbl.gov/>) and reanalysis climatic
241 data from Climatic Research Unit (CRU, Harris et al., 2013) to fill the missing
242 environmental data. To sum up, parameters for various ecosystem types in table 2 were
243 the final results of our parameterization. Model parameterization was conducted for
244 ecosystem types including boreal forest, temperate coniferous forest, temperate
245 deciduous forest, and grassland using SCE-UA-R. Tropical forest and wet tundra used
246 a trial-and-error method to adjust parameters letting simulation results best fit the lab
247 data. Due to limited data availability, we assumed temperate evergreen broadleaf forest
248 having the same parameters as temperate deciduous forest.

249

250 **2.4 Data Organization**

251 To get spatially and temporally explicit estimates of CO consumption, production
252 and net flux at the global scale, we used the data of land cover, soils, climate and leaf
253 area index (LAI) from various sources at a spatial resolution of 0.5° latitude X 0.5°
254 longitude to drive TEM. The land cover data include potential vegetation distribution
255 (Melillo et al., 1993) and soil texture (Zhuang et al., 2003), which were used to assign
256 vegetation- and texture-specific parameters to each grid cell.

257 For the simulation of the period 1901-2013, monthly air temperature, precipitation,
258 clouds fraction and vapor pressure data sets from CRU were used to estimate the soil
259 temperature, soil moisture and SOC with TEM (Figure 4). Monthly LAI data from TEM
260 were required to simulate soil moisture (Zhuang et al., 2004). During this period time,
261 we used an empirical function of latitude, which was derived from the observed
262 latitudinal distribution of tropospheric carbon monoxide (Badr and Probert, 1994) to
263 calculate CO surface concentrations (equation (7), Potter et al., 1996):

$$C_{CO,air} = 82.267856 + 0.8441503L + 1.55934 \times 10^{-2}L^2 + 2.37 \times 10^{-5}L^3 - 2.3 \times 10^{-6}L^4$$

264 Where $C_{CO,air}$ is the derived surface CO concentration (ppbv), L represents
265 latitude which is negative degrees for southern hemisphere and positive degrees for
266 northern hemisphere. We also used the transient atmospheric CO data from MOPITT



267 satellite during 2000-2013 (Figure 5). We averaged day-time and night-time monthly
268 mean retrieved CO surface level 3 data (variables mapped on 0.5° latitude X 0.5°
269 longitude grid scales with monthly time step, Gille, 2013) to represent the CO surface
270 concentration level in each month. The missing pixels were fixed by the average of
271 pixels which had values and were inside 1.5 times of the distance between this missing
272 pixel and the nearest pixel with values. These global mean values shown in Figure 5 do
273 not include ocean surfaces, thus there are differences between our surface CO
274 concentration results and Yoon and Pozzer's report in 2014, which is as low as 99.8ppb.
275 From 2014 to 2100, we used Intergovernmental Panel on Climate Change (IPCC) future
276 climate scenarios from Representative Concentration Pathways (RCPs) climate forcing
277 data sets RCP2.6, RCP4.5 and RCP8.5 (Figure 6). Since RCPs did not have water
278 vapor pressure data, we use the specific humidity and sea level air pressure from the
279 RCPs and elevation of surface to estimate the monthly surface vapor pressure data
280 (Seinfeld & Pandis, 2006).

281

282 **2.5 Model Experiment Design**

283 We conducted two core simulations and eight sensitivity test simulations in
284 historical period. The two core simulations were driven with CO surface concentrations
285 estimated from an empirical function of latitude (experiment E1) for the period 1901-
286 2013 and with transient CO surface concentrations from MOPITT satellite data
287 (experiment E2) for the period 2000-2013, respectively. Eight sensitivity simulations
288 were driven with constant CO surface concentrations $\pm 30\%$, SOC $\pm 30\%$, precipitation
289 $\pm 20\%$ and air temperature $\pm 3^\circ\text{C}$ for each pixel during 1999-2000 (E3). For the 21st
290 century, we conducted simulations driven with climate data of RCP2.6, RCP4.5 and
291 RCP8.5 to examine the responses of CO flux to changing climates (E4).

292

293 **3. Results**

294 **3.1 Site Evaluation**

295 Both the magnitude and variation of the simulated soil temperature and moisture
296 from cold area to warm area compared well to the observations (Figure. 2). The



297 magnitude of simulated CO flux is highly correlated with the observations (r is about 0.5,
298 p -value < 0.001 , Figure 3, a2, b2 ,c2 ,d2). Root mean square error (RMSE) of the
299 simulated CO flux for all sites is below $1.5 \text{ mg CO m}^{-2} \text{ day}^{-1}$. RMSE for site No. 7 is
300 bigger than $2.0 \text{ mg CO m}^{-2} \text{ day}^{-1}$ when compared with transparent chamber
301 observations. For boreal forest site, we only have 8 acceptable points in 1994 and 1996
302 (Figure 3c2).

303 **3.2 Global Soil CO Dynamics During 1901-2013**

304 For the simulation with constant CO surface concentrations (E1) during 1901-
305 2013, the estimated mean soil CO consumption, production and net flux (positive
306 direction is from soil to atmosphere) are -141 , 32 and $-108 \text{ Tg CO yr}^{-1}$, respectively. In
307 the long-term simulations, annual soil CO fluxes vary slightly. The annual soil CO
308 consumption, production and net flux vary within 10% during the period (Figure 8a).
309 Consumption is about 4 times larger than production. The highest rates of consumption
310 and production are located in areas close to the equator, and consumption from areas
311 such as eastern US, Europe and eastern Asia also has large rates ($> -1000 \text{ mg m}^{-2} \text{ yr}^{-1}$)
312 (Figure 7a, b). Globally soils serve as atmospheric CO sink (Figure 7c). Some areas,
313 such as western US and southern Australia, are CO sources, all of which are grassland
314 or experiencing dry climate. The latitudinal distributions of consumption, production and
315 net flux rates share the same spatial pattern. Around 20°S - 20°N and 20 - 60°N are the
316 largest and second largest areas for production and consumption, while the 45°S - 45°N
317 area accounts for nearly 90% of total consumption and production (Figure 9a, Table 3).
318 The Southern and Northern Hemispheres consume 42% and 58% of the total
319 consumption, and produce 41% and 59% of total production, respectively (Table 3).
320 Tropical evergreen forests are the largest sinks, consuming 66 Tg CO yr^{-1} , and tropical
321 savanna and deciduous forest are second and third largest sinks, consuming a total of
322 27 Tg CO yr^{-1} (Table 4). These three ecosystems account for 66% of the total
323 consumption. Tropical evergreen forests are also the largest source of soil CO
324 production, producing 15 Tg CO yr^{-1} , while tropical savanna have a considerable
325 production 6 Tg CO yr^{-1} (Table 4). Moreover, tropical areas, including forested wetlands,
326 forested floodplain and evergreen forests, are most efficient for CO consumption,



327 ranging from -10 to -12 $\text{mg CO m}^{-2} \text{ day}^{-1}$. They are also the most efficient for CO
328 production at over 2 $\text{mg CO m}^{-2} \text{ day}^{-1}$ (Table 3).

329 For the simulation with transient atmospheric CO surface concentrations (E2)
330 during 2000-2013, the mean annual global soil consumption increases to -187 Tg CO
331 yr^{-1} , and areas near the equator become large sinks for atmospheric CO together with
332 eastern US, Europe, and eastern Asia (Figure 7) due to the heavy atmospheric CO
333 burden over these areas (Figure 5a). The annual consumption and net flux trends follow
334 the atmospheric CO concentration trends (Figure 5b, Figure 8b), with a small
335 interannual variability ($<10\%$). The latitudinal distributions of soil CO fluxes for E1 and
336 E2 are similar but E2's CO fluxes magnitudes are larger than E1's and around 30°N of
337 E2's distribution shows another peak of CO consumption, due to the high atmospheric
338 CO concentration over eastern Asia (Figure 5a, Figure 9b). The consumption between
339 45°S - 45°N increases by 35% , to -137 Tg CO yr^{-1} , which is 73% of the global total
340 annual consumption. Consumption rates of high latitude areas (45°N North) do not
341 change significantly (Figure 7, 9, Table 3), and the annual consumption only increases
342 by 10% , thus the portion of soil CO sinks in northern high latitudes decreases from 12%
343 to 10% of the global total.

344

345 **3.3 Global Soil CO Dynamics During 2014-2100**

346 Using the constant atmospheric CO, the estimated annual mean soil CO
347 consumptions for the period 2014-2100 are -162 , -174 and -194 Tg CO yr^{-1} while
348 estimated annual mean soil productions are 36 , 39 and 44 Tg CO yr^{-1} for RCP2.6, 4.5
349 and 8.5 scenarios, respectively. The net fluxes are -118.06 , -117.31 and -115.13 Tg
350 CO yr^{-1} at the beginning 10 years of the 21st century, and will reach -127.17 , -144.99
351 and -187.25 Tg CO yr^{-1} at the end of the 21st century for RCP2.6, RCP4.5 and RCP8.5
352 scenarios, respectively (Figure 11). Global distribution patterns of CO consumption,
353 production and net flux are similar to the 20th century but there are significant
354 differences among RCP2.6 RCP4.5 and 8.5 scenarios on areas near the equator, flux
355 rates increasing from RCP2.6 to 8.5. Areas near the equator and eastern Asia become
356 big sinks of atmospheric CO, while northeastern US becomes a small source (Figure
357 10). The consumption has relatively fast growth rates during the 21st century (Figure 11).



358 Furthermore, there are significant trends of increasing consumption, production and net
359 flux for nearly all scenarios. The rate ranges of increasing of consumption, production,
360 and net flux are -0.15 to -1.23, 0.04 to 0.3, and -0.12 to 0.94 Tg CO yr⁻², respectively
361 (Figure 11). These increasing trends are similar to air temperature increasing trends
362 (Figure 6).

363

364 4. Discussion

365 4.1 Comparison with Other Studies

366 Previous studies estimated a large range of global CO consumption from -16 to -
367 636 Tg CO yr⁻¹. Our estimates are -132 to -154 Tg CO yr⁻¹ for the 20th century and -180
368 to -197 Tg CO yr⁻¹ for 2000-2013 using MOPITT satellite CO surface concentration data.
369 Previous studies also provide a large range for CO production from 0 to 7.6 mg m⁻² day⁻¹
370 (reviewed in Pihlatie et al., 2016). Our results showed averaged CO production
371 ranging from 0.01 to 2.29 mg m⁻² day⁻¹. The large uncertainty of these estimates is
372 mainly due to a different consideration of the microbial activities, the depth of the soil,
373 and the parameters in the model. In contrast to the estimates of -16 to -57 Tg CO yr⁻¹
374 which were based on top 5 cm soils (Potter et al., 1996), our estimates considered
375 30cm soils, just as used in Whalen & Reeburgh (2001). In addition, we used a thinner
376 layer division (1cm each layer) for diffusion process, and used the Crank-Nicolson
377 method solving partial differential equations to avoid time step influences. We also
378 included microbial CO oxidation process to remove the CO from soils and the effects of
379 soil moisture, soil temperature, vegetation type and soil CO substrate on microbial
380 activities. Besides, our soil thermal, soil hydrology and carbon and nitrogen dynamics
381 simulated in TEM provide carbon substrate spatially and temporally for estimating soil
382 CO dynamics (Bonan, 1996; Zhuang et al., 2001, 2003, 2004, 2007). Overall, although
383 a few previous studies have examined the long-term impacts of climate, land use and
384 nitrogen depositions on CO dynamics (Chan & Steudler, 2006, Pihlatie et al., 2016),
385 global prediction of soil CO dynamics still have a large uncertainty.

386

387 4.2 Major Controls to Soil CO Dynamics



388 Eight sensitivity tests have been conducted for the 1999-2000 period, including
389 changing atmospheric CO by $\pm 30\%$, SOC by $\pm 30\%$, precipitation by $\pm 30\%$ and air
390 temperature by $\pm 3^\circ\text{C}$ for each pixel (Table 5). Soil CO consumption is most sensitive
391 (changing 29%) to air temperature while production is most sensitive (changing up to
392 36%) to both air temperature and SOC (30%). The net CO fluxes have the similar
393 sensitivities to consumption, because consumption is normally much larger than CO
394 production so that it will determine the dynamics of the net flux. Annual CO consumption,
395 production and net flux follow the change of air temperature (Table 5), which explains
396 the small increasing trends after the 1960s, the significant increasing trend in the 21st
397 century and the large sinks over tropical areas. Besides, a 30% change in precipitation
398 will not lead to large changes in CO flux ($< 3\%$). SOC did not directly influence CO
399 consumption. Increasing SOC led to an increase in soil CO substrate so implying that
400 more CO in soils can be consumed. CO concentrations will only influence the uptake
401 rate and soil CO substrate concentrations, thus influencing the soil CO consumption
402 rate.

403 Annual CO consumption, production and net flux are significantly correlated with
404 air temperature and soil temperature, due to increasing microbial activities ($R > 0.91$
405 globally). Specifically, annual CO production is strongly correlated with annual mean
406 SOC. The annual mean SOC follows air temperature trends (Figure 4) as CO flux.
407 Consumption has low correlations with annual precipitation and soil moisture, especially
408 at 45°N - 45°S (Table 6). The soil moisture is significantly influenced by temperature
409 since increasing temperature would result in higher evapotranspiration. In contrast, the
410 monthly consumption and production are correlated with the precipitation and soil
411 moisture in the Northern Hemisphere ($R > 0.85$), which contains over 53% of the global
412 soil CO consumption (Table 3). Meanwhile, the monthly CO flux is still well correlated
413 with air temperature and soil moisture. Monthly CO flux has low correlations with SOC
414 because the soil organic carbon will not change greatly within a month. The correlation
415 between annual soil CO consumption and atmospheric CO concentration is 0.91 at the
416 global scale because the atmospheric CO concentration, air temperature, soil
417 temperature dominate the annual consumption rate. At monthly step, this correlation is -
418 0.48 because global atmospheric CO concentrations are high in winter and low in



419 summer while the simulated soil CO consumption shows an opposite monthly
420 variation (Table 6, Figure 12), suggesting that other factors such as precipitation, air
421 temperature, and soil temperature are major controls for monthly CO fluxes.

422

423 **4.3. Model Uncertainties & Limitations**

424 Due to the lack of long-period observational data of CO flux and associated
425 environmental factors, the model parameterization using SCE-UA-R method can only
426 be done for 4 ecosystem types including boreal forest, temperate coniferous forest,
427 temperate deciduous forest and grassland, with RMSE ranging from 0.56 to 1.47 mg m⁻²
428 day⁻¹. Tropical forest calibration is only conducted using a very limited amount of lab
429 experiment data, but tropical areas are hotspots for CO soil-atmosphere exchange.
430 Besides, tropical forest SOC for top 30cm can be really high according to observations.
431 TEM model may underestimate the top 30cm SOC, which will underestimate production
432 rates, especially in tropical region. The large deviation for tropical savanna (which is
433 mosaic of tropical forest and grassland ecosystems) may be due to using outside air
434 temperature to represent inside air temperature of transparent chamber observations
435 (Varella et al., 2004), and uncertain tropical forest parameterization. We used the
436 conclusion from van Asperen et al. (2015) and only considered the thermal-degradation
437 process for CO production. Photo-degradation process and biological formation process
438 were not considered due to lacking understanding of these processes. Although we
439 focused on natural ecosystems in this study, land-use change, agriculture activity, and
440 nitrogen deposition also affect the soil CO consumption and production (King, 2002;
441 Chan & Steudler, 2006). For instance, soil CO consumption in agriculture ecosystems is
442 0 to 9 mg CO m⁻² day⁻¹ in Brazil (King & Hungria, 2002). We used grass land or forest
443 ecosystem to represent agriculture areas in CODM module. Our future study shall
444 include these processes and factors.

445

446 **5. Conclusions**

447 We analyzed the magnitude, spatial pattern, and the controlling factors of
448 atmosphere-soil CO exchange at the global scale for the 20th and 21st centuries using



449 a calibrated process-based biogeochemistry model. Major processes include
450 atmospheric CO diffusion into soils, microbial oxidation removal of CO, and CO
451 production through chemical reaction. We found that air temperature and soil
452 temperature play a dominant role in determining annual soil CO consumption and
453 production while precipitation, air temperature, and soil temperature are the major
454 controls for the monthly consumption and production. Atmospheric CO concentrations
455 will be important for annual CO consumption. We estimated that the global annual CO
456 consumption, production and net flux for the 20th century are 132-154, 29-36 and 112-
457 119 Tg CO yr⁻¹, respectively, when using a constant atmospheric CO concentration. The
458 CO consumption reaches 180-197 Tg CO yr⁻¹ during 2000-2013 when using
459 atmospheric CO concentrations observed by the MOPITT satellite. Tropical evergreen
460 forest, savanna and deciduous forest areas are the largest sinks accounting for 66% of
461 the total CO consumption, while the Northern Hemisphere consumes 60% of the global
462 total. During the 21st century, the predicted net CO flux will reach 126-150 Tg CO yr⁻¹ in
463 the 2090s, primarily because of increasing air temperature. The areas near the equator,
464 eastern Asia, Europe and eastern US will become the sink hotspots because they have
465 warm and moist soils. This study calls for long-period observations of CO flux for
466 various ecosystem types to improve models. The effects of land-use change, agriculture
467 activities, nitrogen deposition, photo-degradation and biological formation shall also be
468 considered to improve future quantification of soil CO fluxes.

469

470

471 **Acknowledgment**

472 This study is supported through projects funded to Q.Z. by Department of Energy
473 (DE-SC0008092 and DE-SC0007007) and the NSF Division of Information and
474 Intelligent Systems (NSF-1028291). The supercomputing resource is provided by
475 Rosen Center for Advanced Computing at Purdue University. We acknowledge Dr.
476 Stephen C. Whalen made the observational CO flux data available to this study. We are
477 also grateful to University of Tuscia (dep. DIBAF), Italy, and their affiliated members, for
478 their help and the use of their field data.

479 **References:**

- 480 Badr, O., & Probert, S. D.: Carbon monoxide concentration in the Earth's atmosphere. *Applied Energy*,
481 doi:10.1016/0306-2619(94)90035-3, 1994
- 482 Badr, O., & Probert, S. D.: Sinks and environmental impacts for atmospheric carbon monoxide, *Applied*
483 *Energy*. doi:10.1016/0306-2619(95)98803-A, 1995
- 484 Bartholemew, G.W., Alexander, M.: Soils as a sink for atmospheric carbon monoxide, *Science* 212, 1389-
485 1391, doi:10.1126/science.212.4501.1389, 1981
- 486 Bartholomew, G. W., & Alexander, M.: Notes. Microorganisms responsible for the oxidation of carbon
487 monoxide in soil. *Environmental Science & Technology*. American Chemical Society (ACS),
488 doi:10.1021/es00099a013, 1982
- 489 Bender, M., & Conrad, R.: Microbial oxidation of methane, ammonium and carbon monoxide, and
490 turnover of nitrous oxide and nitric oxide in soils, *Biogeochemistry*, Springer Nature,
491 doi:10.1007/bf00002813, 1994
- 492 Bergamaschi, P., Hein, R., Heimann, M., & Crutzen, P. J.: Inverse modeling of the global CO cycle: 1.
493 Inversion of CO mixing ratios, *Journal of Geophysical Research: Atmospheres*,
494 doi:10.1029/1999jd900818, 2000
- 495 Bonan, G.: A Land Surface Model (LSM Version 1.0) for Ecological, Hydrological, and Atmospheric
496 Studies: Technical Description and User's Guide, UCAR/NCAR, doi:10.5065/d6df6p5x, 1996
- 497 Bruhn, D., Albert, K. R., Mikkelsen, T. N., & Ambus, P.: UV-induced carbon monoxide emission from living
498 vegetation. *Biogeosciences*, Copernicus GmbH, doi:10.5194/bg-10-7877-2013, 2013
- 499 Castellanos, P., Marufu, L. T., Doddridge, B. G., Taubman, B. F., Schwab, J. J., Hains, J. C., ...
500 Dickerson, R. R.: Ozone, oxides of nitrogen, and carbon monoxide during pollution events over the
501 eastern United States: An evaluation of emissions and vertical mixing, *Journal of Geophysical Research*
502 *Atmospheres*, 116(16), doi:10.1029/2010JD014540, 2011
- 503 Chan, A. S. K., & Stuedler, P. A.: Carbon monoxide uptake kinetics in unamended and long-term
504 nitrogen-amended temperate forest soils. *FEMS Microbiology Ecology*, 57(3), 343–354,
505 doi:10.1111/j.1574-6941.2006.00127.x, 2006
- 506 Conrad, R., & Seiler, W.: Role of Microorganisms in the Consumption and Production of Atmospheric
507 Carbon Monoxide by Soil. *Appl. Environ. Microbiol.*, 40(3), 437–445. Retrieved from
508 <http://aem.asm.org/cgi/content/abstract/40/3/437>, 1980
- 509 Conrad, R., & Seiler, W.: Arid soils as a source of atmospheric carbon monoxide, *Geophysical Research*
510 *Letters*, doi:10.1029/g1009i012p01353, 1982
- 511 Conrad, R., & Seiler, W.: Characteristics of abiological carbon monoxide formation from soil organic
512 matter, humic acids, and phenolic compounds, *Environmental Science & Technology*, American Chemical
513 Society (ACS), doi:10.1021/es00142a004, 1985



- 514 Conrad, R., Meyer, O., & Seiler, W.: Role of carboxydobacteria in consumption of atmospheric carbon
515 monoxide by soil, *Applied and Environmental Microbiology*, 42(2), 211–215, 1981
- 516 Crutzen, P. J., & Giedel, L. T.: A two-dimensional photochemical model of the atmosphere. 2: The
517 tropospheric budgets of anthropogenic chlorocarbons CO, CH₄, CH₃Cl and the effect of various NO_x
518 sources on tropospheric ozone, *J. Geophys. Res.*, 88(C11), 6641–6661. doi:10.1029/JC088iC11p06641,
519 1983
- 520 Crutzen, P.J.: Role of the tropics in atmospheric chemistry, *The Geophysiology of Amazonia Vegetation*
521 *Climate Interaction* (Dickinson RE, ed.), pp 107–131. John Wiley, New York, 1987
- 522 Daniel, J. S., & Solomon, S.: On the climate forcing of carbon monoxide, *Journal of Geophysical*
523 *Research-Atmospheres*, 103(D11), 13249–13260. doi:10.1029/98JD00822, 1988
- 524 Dee, D. P., Uppala, S. M., Simmons, A. J., Berrisford, P., Poli, P., Kobayashi, S., ... Vitart, F.: The ERA-
525 Interim reanalysis: configuration and performance of the data assimilation system, *Quarterly Journal of*
526 *the Royal Meteorological Society*, doi:10.1002/qj.828, 2011
- 527 Dentener, F., Drevet, J., Lamarque, J. F., Bey, I., Eickhout, B., Fiore, A. M., ... Wild, O.: Nitrogen and
528 sulfur deposition on regional and global scales: A multimodel evaluation, *Global Biogeochemical*
529 *Cycles*, 20(4), doi:10.1029/2005GB002672, 2006
- 530 Derendorp, L., Quist, J. B., Holzinger, R., & Röckmann, T.: Emissions of H₂ and CO from leaf litter of
531 *Sequoiadendron giganteum*, and their dependence on UV radiation and temperature, *Atmospheric*
532 *Environment*, 45(39), 7520–7524. doi:10.1016/j.atmosenv.2011.09.044, 2011
- 533 Duan, Q. Y., Gupta, V. K., & Sorooshian, S.: Shuffled complex evolution approach for effective and
534 efficient global minimization, *Journal of Optimization Theory and Applications*, 76(3), 501–521.
535 doi:10.1007/BF00939380, 1993
- 536 Duggin, J. A., & Cataldo, D. A.: The rapid oxidation of atmospheric CO to CO₂ by soils, *Soil Biology and*
537 *Biochemistry*, 17(4), 469–474, doi:10.1016/0038-0717(85)90011-2, 1985
- 538 Emmons, L. K., Walters, S., Hess, P. G., Lamarque, J.-F., Pfister, G. G., Fillmore, D., ... Kloster, S.:
539 Description and evaluation of the Model for Ozone and Related chemical Tracers, version 4 (MOZART-
540 4), *Geoscientific Model Development*, 3(1), 43–67. doi:10.5194/gmd-3-43-2010, 2010
- 541 Fenchel, T., King, G. M., & Blackburn, T. H.: Bacterial biogeochemistry: the ecophysiology of mineral
542 cycling, *Bacterial biogeochemistry* (p. 307 pp). doi:10.1016/B978-0-12-415836-8.00012-8, 1988
- 543 Ferenci, T., Strom, T., & Quayle, J. R.: Oxidation of carbon monoxide and methane by *Pseudomonas*
544 *methanica*, *Journal of General Microbiology*, 91(1), 79–91. doi:10.1099/00221287-91-1-79, 1975
- 545 Fisher, M. E.: Soil-atmosphere Exchange of Carbon Monoxide in Forest Stands Exposed to Elevated and
546 Ambient CO₂ (Doctoral dissertation), 2003
- 547 Fraser, W. T., Blei, E., Fry, S. C., Newman, M. F., Reay, D. S., Smith, K. A., & McLeod, A. R.: Emission of
548 methane, carbon monoxide, carbon dioxide and short-chain hydrocarbons from vegetation foliage under
549 ultraviolet irradiation, *Plant, Cell and Environment*, 38(5), 980–989. doi:10.1111/pce.12489, 2015



- 550 Funk, D. W., Pullman, E. R., Peterson, K. M., Crill, P. M., & Billings, W. D.: Influence of water table on
551 carbon dioxide, carbon monoxide, and methane fluxes from Taiga Bog microcosms, *Global Biogeochem.*
552 *Cycles*, 8(3), 271–278. doi:10.1029/94gb0122, 1994
- 553 Galbally, I., Meyer, C. P., Wang, Y. P., & Kirstine, W.: Soil-atmosphere exchange of CH₄, CO, N₂O and
554 NO_x and the effects of land-use change in the semiarid Mallee system in Southeastern Australia, *Global*
555 *Change Biology*, 16(9), 2407–2419, doi:10.1111/j.1365-2486.2010.02161.x, 2010
- 556 Gille, J.: MOPITT Gridded Monthly CO Retrievals (Near and Thermal Infrared Radiances) - Version 6
557 [Data set], NASA Langley Atmospheric Science Data Center. doi:10.5067/TERRA/MOPITT/DATA301,
558 2013
- 559 Gödde, M., Meuser, K., & Conrad, R.: Hydrogen consumption and carbon monoxide production in soils
560 with different properties, *Biology and Fertility of Soils*, 32(2), 129–134, doi:10.1007/s003740000226, 2000
- 561 Guthrie, P. D.: The CH₄- CO - OH conundrum: A simple analytic approach, *Global Biogeochemical*
562 *Cycles*, doi:10.1029/gb003i004p00287, 1989
- 563 Hardy, K. R., & King, G. M.: Enrichment of High-Affinity CO Oxidizers in Maine Forest Soil. *Applied and*
564 *Environmental Microbiology*, 67(8), 3671–3676, doi:10.1128/AEM.67.8.3671-3676.2001, 2001
- 565 Harris, I., Jones, P. D., Osborn, T. J., & Lister, D. H.: Updated high-resolution grids of monthly climatic
566 observations - the CRU TS3.10 Dataset, *International Journal of Climatology*, doi:10.1002/joc.3711, 2013
- 567 He, H., & He, L.: The role of carbon monoxide signaling in the responses of plants to abiotic
568 stresses, *Nitric Oxide: Biology and Chemistry / Official Journal of the Nitric Oxide Society*, 42, 40–3.
569 doi:10.1016/j.niox.2014.08.011, 2014
- 570 Heichel, G. H.: Removal of Carbon Monoxide by Field and Forest Soils¹, *Journal of Environment Quality*,
571 *American Society of Agronomy*, doi:10.2134/jeq1973.00472425000200040001x, 1973
- 572 Jobbagy, E. G., & Jackson, R.: The vertical Distribution of soil organic carbon and its relation to climate
573 and vegetation, *Ecological Applications*, 10:2(April), 423–436, doi:10.2307/2641104, 2000
- 574 Jones, R. D., & Morita, R. Y.: Carbon monoxide oxidation by chemolithotrophic ammonium
575 oxidizers, *Canadian Journal of Microbiology*, 29(11), 1545–1551, doi:10.1139/m83-237, 1983
- 576 Khalil, M. A. ., Pinto, J. ., & Shearer, M.: Atmospheric carbon monoxide, *Chemosphere - Global Change*
577 *Science*, Elsevier BV, doi:s1465-9972(99)00053-7,1999
- 578 Khalil, M. A. K., & Rasmussen, R. A.: The global cycle of carbon monoxide: Trends and mass
579 balance, *Chemosphere*, 20(1–2), 227–242, doi:10.1016/0045-6535(90)90098-E, 1990
- 580 King, G. M.: Attributes of Atmospheric Carbon Monoxide Oxidation by Maine Forest Soils, *Appl. Environ.*
581 *Microbiol.*, 65(12), 5257–5264, 1999
- 582 King, G. M.: Characteristics and significance of atmospheric carbon monoxide consumption by soils,
583 *Chemosphere*, 1, 53–63, doi:10.1016/S1465-9972(99)00021-5, 1999a
- 584 King, G. M.: Land use impacts on atmospheric carbon monoxide consumption by soils, *Global*
585 *Biogeochemical Cycles*, 14(4), 1161–1172, doi:10.1029/2000GB001272, 2000



- 586 King, G. M., & Crosby, H.: Impacts of plant roots on soil CO cycling and soil-atmosphere CO
587 exchange, *Global Change Biology*, 8(11), 1085–1093, doi:10.1046/j.1365-2486.2002.00545.x, 2002
- 588 King, G. M., & Hungria, M.: Soil-atmosphere CO exchanges and microbial biogeochemistry of CO
589 transformations in a Brazilian agricultural ecosystem, *Applied and Environmental Microbiology*, 68(9),
590 4480–4485, doi:10.1128/AEM.68.9.4480-4485.2002, 2002
- 591 King, G. M., & Weber, C. F.: Distribution, diversity and ecology of aerobic CO-oxidizing bacteria, *Nature*
592 *Reviews, Microbiology*, 5(2), 107–18, doi:10.1038/nrmicro1595, 2007
- 593 King, J. Y., Brandt, L. A., & Adair, E. C.: Shedding light on plant litter decomposition: advances,
594 implications and new directions in understanding the role of photodegradation, *Biogeochemistry*, 111(1–
595 3), 57–81, doi:10.1007/s10533-012-9737-9, 2012
- 596 Kisselle, K. W., Zepp, R. G., Burke, R. A., De Pinto, A. S., Bustamante, M. M. C., Opsahl, S., ... Viana, L.
597 T.: Seasonal soil fluxes of carbon monoxide in burned and unburned Brazilian savannas, *Journal of*
598 *Geophysical Research Atmospheres*, 107(20), doi:10.1029/2001JD000638, 2002
- 599 Kuhlbusch, T. A., Zepp, R. G., Miller, W. L., & A BURKE, R.: Carbon monoxide fluxes of different soil
600 layers in upland Canadian boreal forests, *Tellus B. Informa UK Limited*, doi:10.1034/j.1600-
601 0889.1998.t01-3-00003.x, 1998
- 602 Lamarque, J. F., Emmons, L. K., Hess, P. G., Kinnison, D. E., Tilmes, S., Vitt, F., ... Tyndall, G. K.: CAM-
603 chem: Description and evaluation of interactive atmospheric chemistry in the Community Earth System
604 Model, *Geoscientific Model Development*, 5(2), 369–411, <https://doi.org/10.5194/gmd-5-369-2012>, 2012
- 605 Lee, H., Rahn, T., & Throop, H.: An accounting of C-based trace gas release during abiotic plant litter
606 degradation, *Global Change Biology*, 18(3), 1185–1195, doi:10.1111/j.1365-2486.2011.02579.x, 2012
- 607 Logan, J. A., Prather, M. J., Wofsy, S. C., & McElroy, M. B.: Tropospheric chemistry - A global
608 perspective, *J. Geophys. Res.*, doi:10.1029/JC086iC08p07210, 1981
- 609 Lu, Y., & Khalil, M. A. K.: Methane and carbon monoxide in OH chemistry: The effects of feedbacks and
610 reservoirs generated by the reactive products, *Chemosphere. Elsevier BV*, doi:10.1016/0045-
611 6535(93)90450-j, 1993
- 612 Luo, M., Read, W., Kulawik, S., Worden, J., Livesey, N., Bowman, K., & Herman, R.: Carbon monoxide
613 (CO) vertical profiles derived from joined TES and MLS measurements, *Journal of Geophysical Research*
614 *Atmospheres*, 118(18), 10601–10613, doi:10.1002/jgrd.50800, 2013
- 615 Moxley, J. M., & Smith, K. A.: Factors affecting utilisation of atmospheric CO by soils, *Soil Biology and*
616 *Biochemistry*, 30(1), 65–79, doi:10.1016/S0038-0717(97)00095-3, 1998
- 617 Myhre, G., Shindell, D., Bréon, F. M., Collins, W., Fuglestedt, J., Huang, J., ... & Nakajima, T.:
618 Anthropogenic and Natural Radiative Forcing. In: *Climate Change 2013: The Physical Science Basis,*
619 *Contribution of Working Group 1 to the Fifth Assessment Report of the Intergovernmental Panel on*
620 *Climate Change. Table, 8, 714, 2013*



- 621 Philip, R., & Novick, K.: AmeriFlux US-MMS Morgan Monroe State Forest [Data set]. AmeriFlux; Indiana
622 University, doi:10.17190/AMF/1246080, 2016
- 623 Pihlatie, M., Rannik, Ü., Haapanala, S., Peltola, O., Shurpali, N., Martikainen, P. J., ... Mammarella, I.:
624 Seasonal and diurnal variation in CO fluxes from an agricultural bioenergy crop, Biogeosciences.
625 Copernicus GmbH, doi:10.5194/bg-13-5471-2016, 2016
- 626 Potter, C. S., Klooster, S. A., & Chatfield, R. B.: Consumption and production of carbon monoxide in soils:
627 A global model analysis of spatial and seasonal variation, Chemosphere, 33(6), 1175–1193,
628 doi:10.1016/0045-6535(96)00254-8, 1996
- 629 Prather, M., and Ehhalt, D.: Atmospheric chemistry and greenhouse gases. Climate Change, 2001: The
630 Scientific Basis (Houghton JT, Ding Y, Griggs DJ, Noguer M, van der Linden PJ, Dai X, Maskell K &
631 Johnson CA, eds), pp. 239–288, Cambridge University Press, Cambridge, UK, 2001
- 632 Prather, M., Derwent, R., Ehhalt, D., Fraser, P., Sanhueza, E. and Zhou, X.: Other trace gases and
633 atmospheric chemistry, Climate Change, 1994. Radiative Forcing of Climate Change (Houghton JT, Meira
634 Filho LG, Bruce J, Hoesung Lee BA, Callander E, Haites E, Harris N & Maskell K, eds), pp. 76–126,
635 Cambridge University Press, Cambridge, UK, 1995
- 636 SALESKA, S. R., DA ROCHA, H. R., HUETE, A. R., NOBRE, A. D., ARTAXO, P. E., & SHIMABUKURO,
637 Y. E.: LBA-ECO CD-32 Flux Tower Network Data Compilation, Brazilian Amazon: 1999-2006, ORNL
638 Distributed Active Archive Center, doi:10.3334/ORNLDAAC/1174, 2013
- 639 Sanderson, M. G., Collins, W. J., Derwent, R. G., & Johnson, C. E.: Simulation of global hydrogen levels
640 using a Lagrangian three-dimensional model, Journal of Atmospheric Chemistry, 46(1), 15–28,
641 doi:10.1023/A:1024824223232, 2003
- 642 Sanhueza, E., Dong, Y., Scharffe, D., Lobert, J. M., & Crutzen, P. J.: Carbon monoxide uptake by
643 temperate forest soils: The effects of leaves and humus layers, Tellus, Series B: Chemical and Physical
644 Meteorology, 50(1), 51–58, doi:10.1034/j.1600-0889.1998.00004.x, 1998
- 645 Schade, G. W., & Crutzen, P. J.: CO emissions from degrading plant matter (II). Estimate of a global
646 source strength, Tellus, Series B: Chemical and Physical Meteorology, 51(5), 909–918,
647 doi:10.1034/j.1600-0889.1999.t01-4-00004.x, 1999
- 648 Scharffe, D., Hao, W. M., Donoso, L., Crutzen, P. J., & Sanhueza, E.: Soil fluxes and atmospheric
649 concentration of CO and CH₄ in the northern part of the Guayana shield, Venezuela, Journal of
650 Geophysical Research-Atmospheres, 95(90), 22475–22480, doi:10.1029/JD095iD13p22475, 1990
- 651 Seiler, W.: In: Krumbein, W.E. (Ed.), Environmental Biogeochemistry and Geomicrobiology, Methods,
652 Metals and Assessment, vol. 3, Ann Arbor Science, Ann Arbor, MI, pp. 773-810, 1987
- 653 Seinfeld, J. H., & Pandis, S. N.: Atmospheric Chemistry and Physics: From Air Pollution to Climate
654 Change, Atmospheric Chemistry and Physics from Air Pollution to Climate Change Publisher New York
655 NY Wiley 1998 Physical Description Xvii 1326 p A WileyInterscience Publication ISBN 0471178152, 51,
656 1–4, doi:10.1080/00139157.1999.10544295, 1998



- 657 Stein, O., Schultz, M. G., Bouarar, I., Clark, H., Huijnen, V., Gaudel, A., ... Clerbaux, C.: On the
658 wintertime low bias of Northern Hemisphere carbon monoxide found in global model
659 simulations, *Atmospheric Chemistry and Physics*, 14(17), 9295–9316, doi:10.5194/acp-14-9295-2014,
660 2014
- 661 Stevenson, D. S., Dentener, F. J., Schultz, M. G., Ellingsen, K., van Noije, T. P. C., Wild, O., ... Szopa, S.:
662 Multimodel ensemble simulations of present-day and near-future tropospheric ozone, *Journal of*
663 *Geophysical Research Atmospheres*, 111(8), doi:10.1029/2005JD006338, 2006
- 664 Suzuki, R.: AmeriFlux US-Prr Poker Flat Research Range Black Spruce Forest [Data set], AmeriFlux;
665 Japan Agency for Marine-Earth Science and Technology, doi:10.17190/AMF/1246153, 2016
- 666 Tan, Z., & Zhuang, Q.: An analysis of atmospheric CH₄ concentrations from 1984 to 2008 with a single
667 box atmospheric chemistry model, *Atmospheric Chemistry and Physics Discussions*, Copernicus GmbH,
668 doi:10.5194/acpd-12-30259-2012, 2012
- 669 Tarr, M. a., Miller, W. L., & Zepp, R. G.: Direct carbon monoxide photoproduction from plant
670 matter, *Journal of Geophysical Research*, 100, 11403, doi:10.1029/94JD03324, 1995
- 671 Taylor, J. A., Zimmerman, P. R., & Erickson, D. J.: A 3-D modelling study of the sources and sinks of
672 atmospheric carbon monoxide, *Ecological Modelling*, 88(1–3), 53–71, doi:10.1016/0304-3800(95)00069-
673 0, 1996
- 674 van Asperen, H., Warneke, T., Sabbatini, S., Nicolini, G., Papale, D., & Notholt, J.: The role of photo- and
675 thermal degradation for CO₂ and CO fluxes in an arid ecosystem, *Biogeosciences*,
676 12(13), 4161–4174, doi:10.5194/bg-12-4161-2015, 2015
- 677 Varella, R. F., Bustamante, M. M. C., Pinto, A. S., Kisselle, K. W., Santos, R. V., Burke, R. A., ... Viana, L.
678 T.: Soil fluxes of CO₂, CO, NO, and N₂O from an old pasture and from native Savanna in
679 Brazil, *Ecological Applications*, 14(4 SUPPL.), doi:10.1890/01-6014, 2004
- 680 Vreman, H. J., Wong, R. J., & Stevenson, D. K.: Quantitating carbon monoxide production from heme by
681 vascular plant preparations in vitro, *Plant Physiology and Biochemistry*, 49(1), 61–68,
682 doi:10.1016/j.plaphy.2010.09.021, 2011
- 683 Wesely, M. L.: Parameterization of surface resistances to gaseous dry deposition in regional-scale
684 numerical models. *Atmospheric Environment* (1967), Elsevier BV, doi:10.1016/0004-6981(89)90153-4,
685 1989
- 686 Wesely, M., & Hicks, B.: A review of the current status of knowledge on dry deposition. *Atmospheric*
687 *Environment*, 34, 2261–2282, doi:10.1016/S1352-2310(99)00467-7, 2000
- 688 Whalen, S. C., & Reeburgh, W. S.: Carbon monoxide consumption in upland boreal forest soils, *Soil*
689 *Biology and Biochemistry*, 33(10), 1329–1338, doi:10.1016/S0038-0717(01)00038-4, 2001
- 690 Yonemura, S., Kawashima, S., & Tsuruta, H.: Carbon monoxide, hydrogen, and methane uptake by soils
691 in a temperate arable field and a forest, *Journal of Geophysical Research*, 105(DII), 14347,
692 <https://doi.org/10.1029/1999JD901156>, 2000



- 693 Yoon, J., & Pozzer, A.: Model-simulated trend of surface carbon monoxide for the 2001-2010
694 decade, *Atmospheric Chemistry and Physics*, 14(19), 10465–10482, doi:10.5194/acp-14-10465-2014,
695 2014
- 696 Zepp, R. G., Miller, W. L., Tarr, M. A., Burke, R. A., & Stocks, B. J.: Soil-atmosphere fluxes of carbon
697 monoxide during early stages of postfire succession in upland Canadian boreal forests, *Journal of*
698 *Geophysical Research-Atmospheres*, 102(D24), 29301–29311, doi:10.1029/97jd01326, 1997
- 699 Zhuang, Q., McGuire, A. D., Melillo, J. M., Klein, J. S., Dargaville, R. J., Kicklighter, D. W., ... Hobbie, J.
700 E.: Carbon cycling in extratropical terrestrial ecosystems of the Northern Hemisphere during the 20th
701 century: A modeling analysis of the influences of soil thermal dynamics, *Tellus, Series B: Chemical and*
702 *Physical Meteorology*, 55(3), 751–776, doi:10.1034/j.1600-0889.2003.00060.x, 2003
- 703 Zhuang, Q., Melillo, J. M., Kicklighter, D. W., Prinn, R. G., McGuire, A. D., Steudler, P. A., ... Hu, S.:
704 Methane fluxes between terrestrial ecosystems and the atmosphere at northern high latitudes during the
705 past century: A retrospective analysis with a process-based biogeochemistry model, *Global*
706 *Biogeochemical Cycles*, 18(3), doi:10.1029/2004GB002239, 2004
- 707 Zhuang, Q., Melillo, J. M., McGuire, A. D., Kicklighter, D. W., Prinn, R. G., Steudler, P. A., ... Hu, S.: Net
708 emissions of CH₄ and CO₂ in Alaska: Implications for the region's greenhouse gas budget, *Ecological*
709 *Applications*, 17(1), 203–212, doi:10.1890/1051-0761(2007)017[0203:NEOCAC]2.0.CO;2, 2007
- 710 Zhuang, Q., Romanovsky, V. E., & McGuire, a. D.: Incorporation of a permafrost model into a large-scale
711 ecosystem model: Evaluation of temporal and spatial scaling issues in simulating soil thermal
712 dynamics, *Journal of Geophysical Research*, 106, 33649, doi:10.1029/2001JD900151, 2001
- 713 Zhuang, Q., Chen, M., Xu, K., Tang, J., Saikawa, E., Lu, Y., ... McGuire, A. D.: Response of global soil
714 consumption of atmospheric methane to changes in atmospheric climate and nitrogen deposition, *Global*
715 *Biogeochemical Cycles*, doi:10.1002/gbc.20057, 2013

716

Table 1. Model parameterization sites for thermal and hydrology modules (site No. 1-4) and for CODM module (site No. 5-13)

No.	Site Name	Location	Vegetation	Driving Climate	Observed Data	Source and Comments
1	Poker Flat Research Range Black Spruce Forest (US_PRR)	147°29'W/65°7'N	Boreal Evergreen Needle Leaf Forests	Site Observation & ERA Interim	Soil Temperature and Moisture of 2011-2014	Suzuki (2016)
2	Morgan Monroe State Forest (US_MMFS)	86°25'W/39°19'N	Temperate Deciduous Broadleaf Forests	Site Observation & ERA Interim	Soil Temperature and Moisture of 1999-2014	Philip and Novick (2016)
3	Santarem, Tapajós National Forest (STM_K83)	54°56'W/3°3'S	Tropical Moist Forest	Site Observation & ERA Interim	Soil Temperature and Moisture of 2000-2004	SALESKA et al. (2013)
4	Bananal Island Site (TOC_BAN)	50°08'W/9°49'S	Tropical Forest- Savanna	Site Observation & ERA Interim	Soil Temperature and Moisture of 2003-2006	SALESKA et al. (2013)
5	Eastern Finland (EF)	27°14'E/63°9'N	Boreal Grassland	Site Observation & ERA Interim	CO flux of April-November, 2011	Phillatte et al. (2016)
6	Viterbo, Italy (VI)	11°55'E/42°22'N	Mediterranean Grassland	Site Observation & ERA Interim	CO flux of August, 2013	van Asperen et al. (2015)
7	Brasilia, Brazil (BB)	47°51'W/15°56'S	Tropical Savanna	Site Observation & CRU	CO flux of October 1999 to July 2001	Varella et al. (2004)
8	Orange County, North Carolina (OC)	79°7'W/35°58'N	Temperate Coniferous Forest	AMF_US-DK3 2002-2003	CO flux of March 2002 to March 2003	Fisher (2003)
9	Tsukuba Science City, Japan (TSC)	140°7'E/36°01'N	Temperate Mixed Forest	Site Observation & ERA Interim	CO flux of July 1996 to September 1997	Yonemura et al. (2000)
10	Manitoba, Canada (CBS)	96°44'W/56°09'N	Boreal Pine Forest	Site Observation & AMF_CA-Man	CO flux of June-August, 1994	Kuhlbusch et al. (1998)
11	Scotland, U.K. (SUK)	3°12'W/55°51'N	Temperate Deciduous Forests	ERA Interim 1995	CO flux of 1995	Moxley and Smith (1998)
12	Alaska, USA (AUS)	147°41'W/64°52' N	Boreal wetland	CRU 1991	CO flux of Lab Experiment, 1991	Funk et al. (1994)
13	Guayana Shield Bolivar State, Venezuela (GBV)	62°57'W/7°51'N	Tropical Smi-deciduous Forest	CRU 1985	CO flux of Lab Experiment, 1985	Schaffte et al. (1990)

717



718

719 **Table 2.** Ecosystem-specific parameters in the CODM module^a

Ecosystem Type	k_{CO} ($\mu\text{l CO l}^{-1}$)	V_{max} ($\mu\text{g CO g}^{-1}\text{h}^{-1}$)	T_{ref} ($^{\circ}\text{C}$)	Q_{10} (Unitless)	M_{min}^p ($\frac{p}{v}$)	M_{max}^p ($\frac{p}{v}$)	M_{opt}^p ($\frac{p}{v}$)	E_{SOC}	F_{SOC}^g ($\frac{g}{g}$)	$\frac{E_{d-ref}}{R}$ (K)	PM_{ref}^p ($\frac{p}{v}$)	PT_{ref} ($^{\circ}\text{C}$)
1 Alpine Tundra & Polar Desert	36.00	0.78	4.00	1.80	0.10	1.00	0.55	3.00	0.33	7700	0.25	30.00
2 Wet Tundra	36.00	0.70	4.00	1.80	0.25	1.00	0.55	3.00	0.42	7700	0.25	30.00
3 Boreal Forest	27.34	1.18	9.81	1.60	0.15	0.64	0.53	2.98	0.50	8827	0.35	26.99
4 Temperate Coniferous Forest	42.64	2.15	6.90	1.87	0.02	0.96	0.53	2.86	0.50	8404	0.38	31.52
5 Temperate Deciduous Forest	40.16	2.43	8.54	1.51	0.17	0.81	0.51	2.45	0.50	8801	0.35	37.44
6 Grassland	42.41	0.49	11.27	1.65	0.16	0.82	0.51	3.09	0.42	14165	0.24	12.29
7 Xeric Shrublands	8.00	0.30	4.00	1.50	0.10	1.00	0.55	3.00	0.33	7700	0.25	30.00
8 Tropical Forest	45.00	2.00	4.00	1.50	0.10	1.00	0.55	3.80	0.50	14000	0.50	18.00
9 Xeric Woodland	8.00	0.30	4.00	1.50	0.10	1.00	0.55	3.00	0.50	7700	0.25	30.00
10 Temperate Evergreen Broadleaf Forest	40.16	2.43	8.54	1.51	0.17	0.81	0.51	2.45	0.50	8801	0.35	37.44
11 Mediterranean Shrubland	45.00	1.50	4.00	1.50	0.10	1.00	0.55	3.00	0.33	7700	0.25	30.00
** Largest Potential Value	51.00	11.1	15.00	2.00	0.30	1.00	0.60	3.80	--	15000	0.60	40.00

^a k_{CO} is the half-saturation constant for soil CO concentration; V_{max} is the specific maximum CO oxidation rate; T_{ref} is the reference temperature to account for soil temperature effects on CO consumption; Q_{10} is the an ecosystem-specific Q_{10} coefficient to account for soil temperature effects on CO consumption; M_{min}^p , M_{max}^p , M_{opt}^p are the minimum, optimum, and maximum volumetric soil moistures of oxidation reaction to account for soil moisture effects on CO consumption; E_{SOC} is an estimated nominal CO production factor, similar as Potter et al. (1996) (10^{-4} mg CO $\text{m}^{-2}\text{d}^{-1}$ per g SOC m^{-2}); F_{SOC}^g is a constant fraction of top 20cm SOC compared to total amount of SOC to account for SOC effects on CO production; E_{d-ref}/R is the is the ecosystem-specific activation energy divided by gas constant to account for the reaction rate of production; PM_{ref}^p is the reference moisture to account for soil temperature effects on CO production; PT_{ref} is the reference temperature to account for soil temperature effects on CO production

720
721





722 **Table 3.** Regional soil CO consumption, net flux and production(Tg CO yr⁻¹) during 1901- 2013 (E1) and during
723 2000-2013 withMOPITT data transient CO surface concentration

	South-45°S		45°S-0°		0°-45°N		45°N-North		Global	
	E1 ^a	E2 ^b	E1	E2	E1	E2	E1	E2	E1	E2
Consumption	-0.20	-0.22	-58.36	-75.77	-64.78	-91.66	-17.24	-18.90	-140.58	-186.55
Net flux	-0.12	-0.13	-43.39	-59.34	-51.58	-77.17	-13.27	-14.63	-108.35	-151.27
Production	0.09	0.09	14.98	16.43	13.20	14.49	3.97	4.27	32.23	35.28

724

725 ^aE1 represents the simulation with constant CO surface concentration data;

726 ^bE2 represents the simulation with MOPITT transient CO surface concentration data.

727

728

729

730

731

732

733

734

735

736

737

738

739

740

741

742

743

744

745

746

747 **Table 4.** Global soil CO consumption, net flux and production in different ecosystems during 1901-2013

Vegetation Type	Area (10 ⁶ km ²)	Pixels	Consumption (Tg CO yr ⁻¹)	Net flux (Tg CO yr ⁻¹)	Production (Tg CO yr ⁻¹)
Alpine Tundra & Polar Desert	5.28	3580	-0.95	-0.73	0.22
Wet Tundra	5.24	4212	-1.06	-0.52	0.54
Boreal Forest	12.47	7578	-7.19	-5.53	1.66
Forested Boreal Wetland	0.23	130	-0.13	-0.09	0.04
Boreal Woodland	6.48	4545	-2.40	-1.53	0.88
Non-Forested Boreal Wetland	0.83	623	-0.33	-0.17	0.16
Mixed Temperate Forest	5.25	2320	-6.31	-5.82	0.49
Temperate Coniferous Forest	2.49	1127	-2.78	-2.49	0.29
Temperate Deciduous Forests	3.65	1666	-3.26	-3.02	0.24
Temperate Forested Wetland	0.15	60	-0.22	-0.21	0.01
Tall Grassland	3.63	1567	-1.28	-0.37	0.91
Short Grassland	4.71	2072	-0.93	-0.25	0.68
Tropical Savanna	13.85	4666	-15.83	-10.41	5.42
Xeric Shrubland	14.71	5784	-1.61	-1.33	0.28
Tropical Evergreen Forest	17.77	5855	-66.12	-51.28	14.84
Tropical Forested Wetland	0.55	178	-2.51	-2.05	0.46
Tropical Deciduous Forest	4.69	1606	-11.20	-8.48	2.72
Xeric Woodland	6.85	2387	-6.53	-5.57	0.96
Tropical Forested Floodplain	0.15	50	-0.64	-0.54	0.11
Desert	11.61	4170	-0.49	-0.45	0.05
Tropical Non-forested Wetland	0.06	19	-0.02	-0.01	0.01
Tropical Non-forested Floodplain	0.36	120	-0.20	-0.11	0.09
Temperate Non-Forested Weland	0.34	120	-0.22	-0.10	0.13
Temperate Forested Floodplain	0.10	48	-0.10	-0.10	0.00
Temperate Non-forested Floodplain	0.10	45	-0.04	-0.02	0.01
Wet Savanna	0.16	59	-0.27	-0.21	0.06
Salt Marsh	0.09	35	-0.04	-0.01	0.02
Mangroves	0.12	38	-0.39	-0.32	0.07
Temperate Savannas	6.83	2921	-3.17	-2.63	0.54
Temperate Evergreen Broadleaf	3.33	1268	-3.60	-3.39	0.21
Mediterranean Shrubland	1.47	575	-0.75	-0.60	0.15
Total	133.56	59424	-140.58	-108.35	32.23

748

749

750

751

752

753



754 **Table 5.** Sensitivity of global CO consumption, net flux and production (units are Tg CO yr⁻¹) to changes in
755 atmospheric CO, soil organic carbon (SOC), precipitation (Prec) and air temperature (AT)

	Baseline	CO +30%	CO -30%	SOC +30%	SOC -30%	Prec +30%	Prec -30%	AT +3°C	AT -3°C
Consumption	-147.65	-164.14	-131.12	-175.37	-119.90	-150.72	-143.50	-190.59	-114.83
Change (%)	0.00	-11.17	11.19	-18.78	18.79	-2.08	2.81	-29.09	22.23
Net flux	-113.65	-130.15	-97.12	-131.18	-96.10	-116.97	-109.32	-144.23	-89.58
Change (%)	0.00	-14.51	14.54	-15.42	15.44	-2.92	3.81	-26.90	21.18
Production	33.99	33.99	33.99	44.19	23.80	33.74	34.17	46.36	25.25
Change (%)	0.00	0.00	0.00	30.00	-30.00	-0.75	0.53	36.39	-25.72

756

757

758

759

760

761

762

763

764

765

766

767

768

769

770

771

772

773

774

775

776



777 **Table 6.** Effects of annual and monthly climate precipitation (Prec), air temperature (Tair), soil organic carbon
 778 (SOC), soil temperature (Tsoil), soil moisture (Msoil) and atmospheric CO (CO air) on absolute values of
 779 consumption, production and net flux for different regions and the globe during the 20th Century

		Monthly					Annual				
		North- 45°N	45°N- 0°	0°- 45°S	45°S- South	Global	North- 45°N	45°N- 0°	0°- 45°S	45°S- South	Global
Prec	Consumption	0.91	0.96	0.92	-0.34	0.87	0.65	0.21	0.26	0.13	0.52
	Production	0.91	0.70	0.45	-0.34	0.82	0.63	0.10	0.15	-0.11	0.47
	Net flux	0.91	0.97	0.94	-0.33	0.87	0.65	0.25	0.31	0.32	0.54
Tair	Consumption	0.97	0.98	0.91	0.96	0.95	0.92	0.93	0.88	0.84	0.91
	Production	0.96	0.83	0.72	0.98	0.94	0.92	0.92	0.91	0.95	0.91
	Net Flux	0.97	0.97	0.88	0.90	0.95	0.91	0.92	0.85	0.62	0.91
SOC	Consumption	-0.19	0.07	0.21	-0.01	0.15	0.68	0.90	0.92	0.47	0.92
	Production	-0.19	0.31	0.47	-0.02	0.24	0.72	0.92	0.92	0.50	0.93
	Net Flux	-0.19	0.03	0.14	0.00	0.13	0.67	0.88	0.91	0.38	0.91
Tsoil	Consumption	0.97	0.98	0.92	0.96	0.95	0.94	0.93	0.88	0.85	0.95
	Production	0.97	0.83	0.72	0.98	0.94	0.94	0.92	0.91	0.96	0.95
	Net Flux	0.98	0.97	0.88	0.90	0.95	0.93	0.93	0.86	0.63	0.95
Msoil	Consumption	0.85	0.96	0.92	0.19	0.76	0.03	0.22	0.14	0.26	0.22
	Production	0.85	0.75	0.44	0.14	0.69	-0.02	0.12	0.02	0.05	0.17
	Net Flux	0.84	0.96	0.95	0.25	0.77	0.04	0.26	0.19	0.40	0.24
CO Air	Consumption	-0.66	-0.76	-0.29	0.14	-0.48	0.87	0.88	0.81	0.98	0.91
	Production	-0.70	-0.66	0.08	-0.40	-0.66	-0.36	-0.48	-0.54	-0.44	-0.57
	Net Flux	-0.64	-0.73	-0.35	0.55	-0.41	0.92	0.91	0.88	0.99	0.94

780

781

782

783

784

785

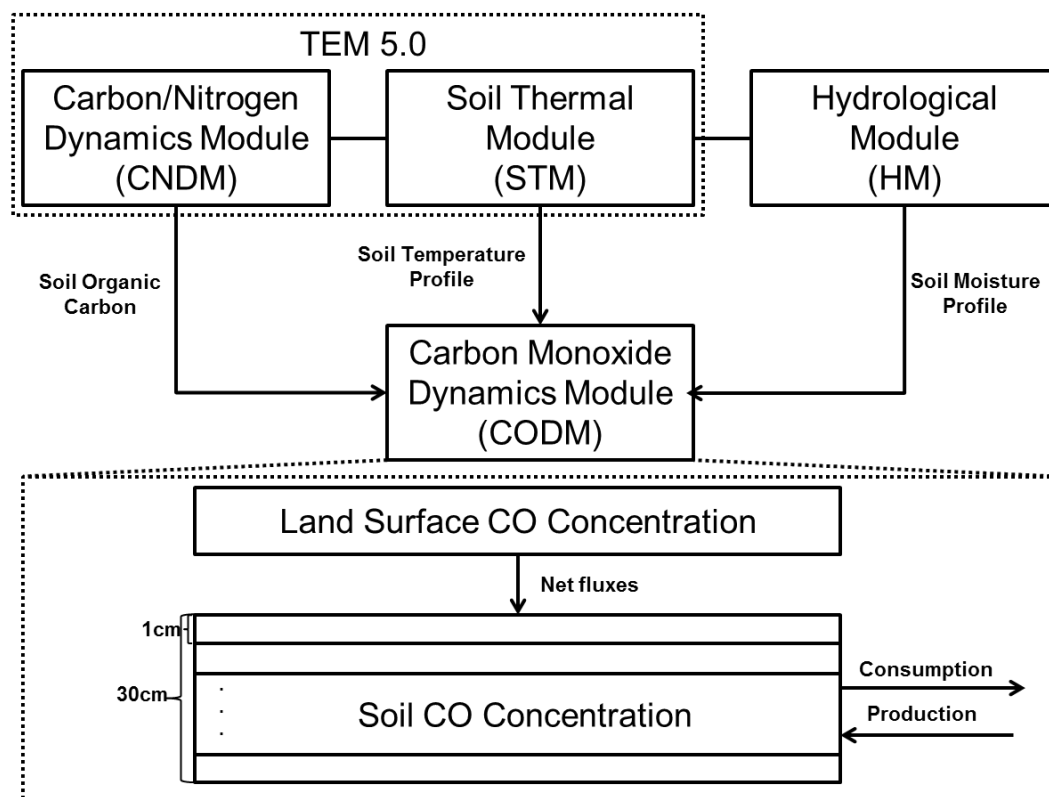
786

787

788

789

790



791

792 **Figure 1. The model framework** includes a carbon and nitrogen dynamics module (CNDM), a soil thermal module (STM)
793 from Terrestrial Ecosystem Model (TEM) 5.0 (Zhuang et al., 2001, 2003), a hydrological module (HM) based on a Land
794 Surface Module (Bonan, 1996; Zhuang et al., 2004), and a carbon monoxide dynamics module (CODM). The detailed
795 structure of CODM includes land surface CO concentration as top boundary and thirty 1 cm thick layers (totally 30 cm)
796 where consumption and production would happen inside.

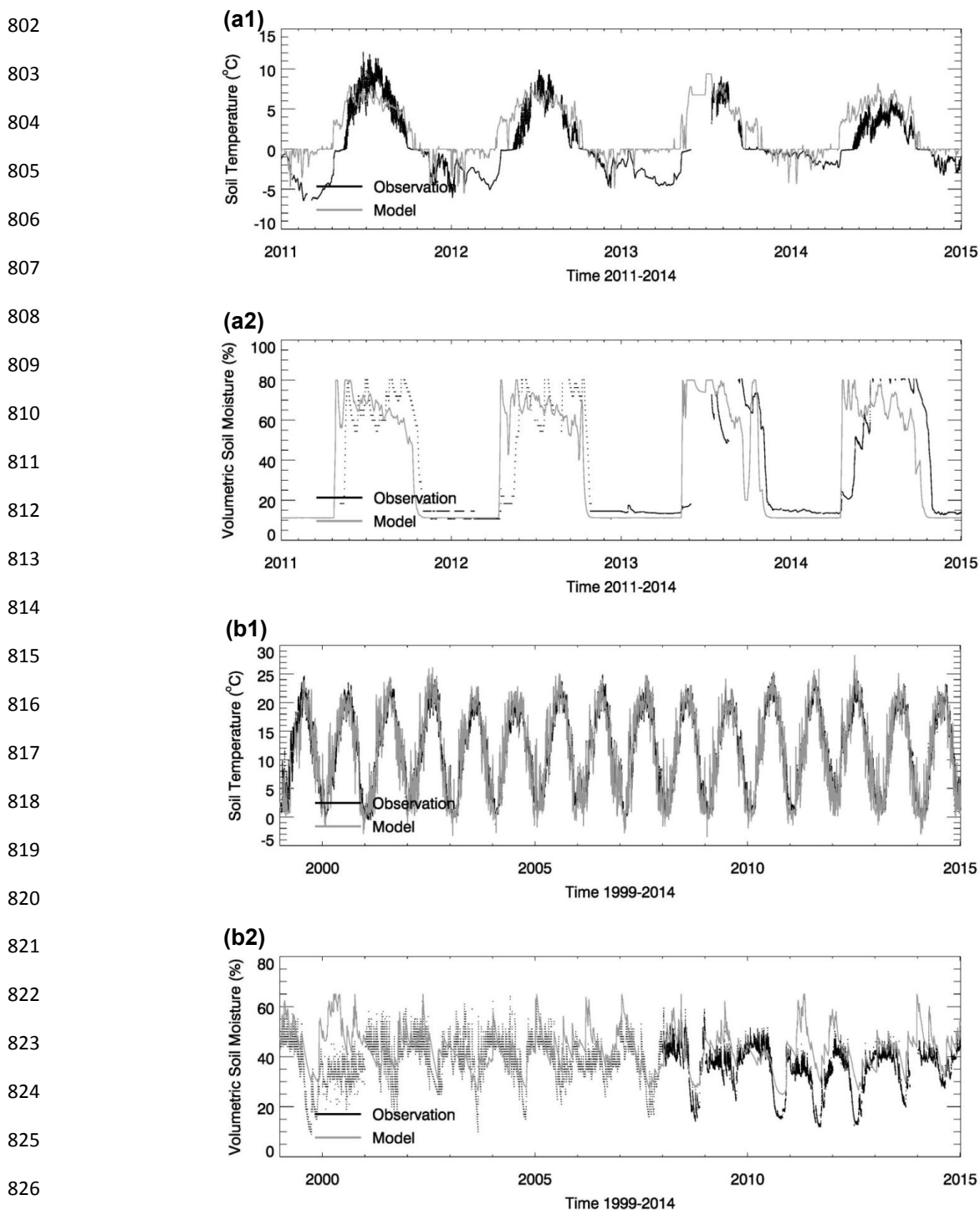
797

798

799

800

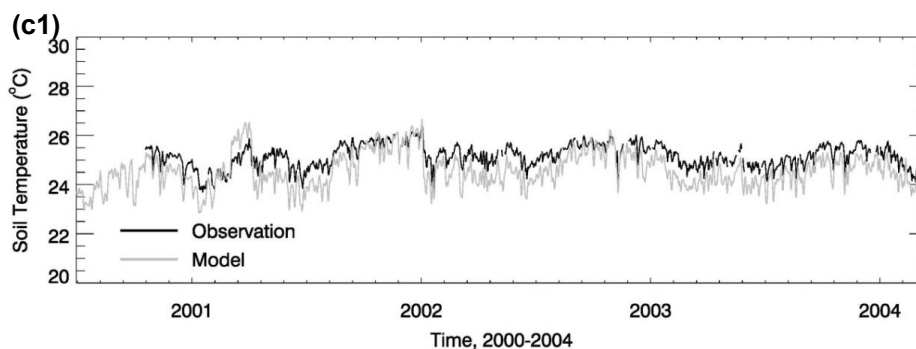
801



827 **Figure 2.** Evaluation of thermal and hydrology module at four sites: (a) Boreal Evergreen Needle Leaf Forests, (b)
828 Temperate Deciduous Broadleaf Forests. (1) shows the soil temperature comparison between model simulations (gray
829 line) and observations (black line) and (2) shows the soil moisture comparison between model simulations (gray line) and
830 observations (black line).



831



832

833

834

835

836

837

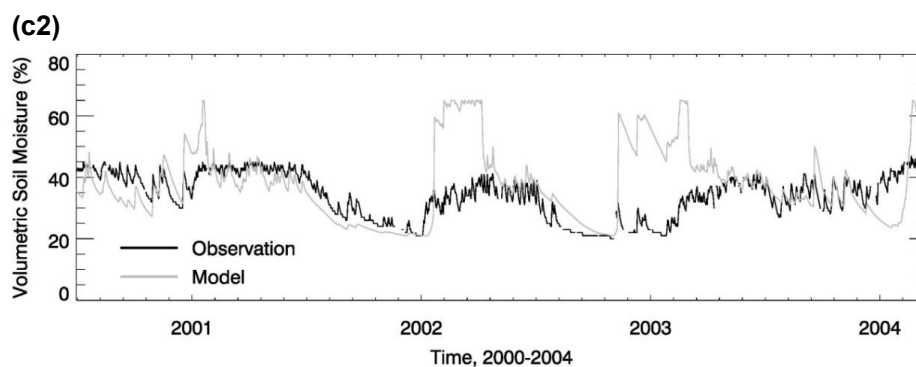
838

839

840

841

842



843

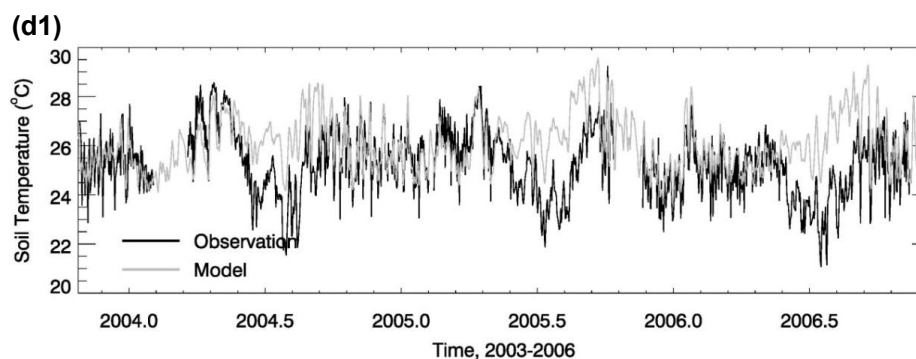
844

845

846

847

848



849

850

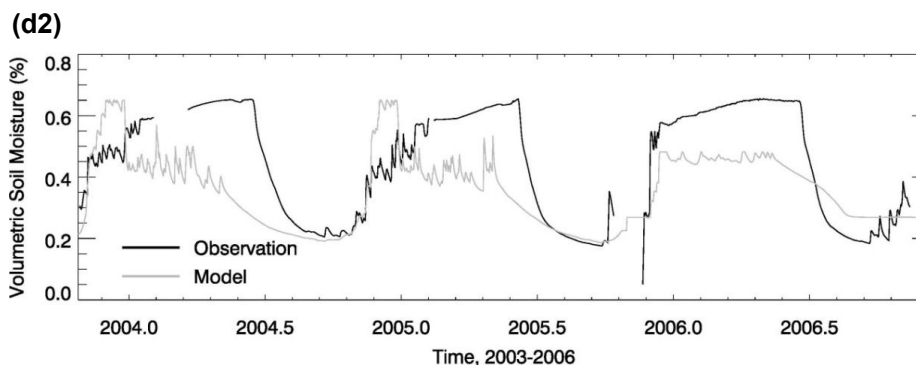
851

852

853

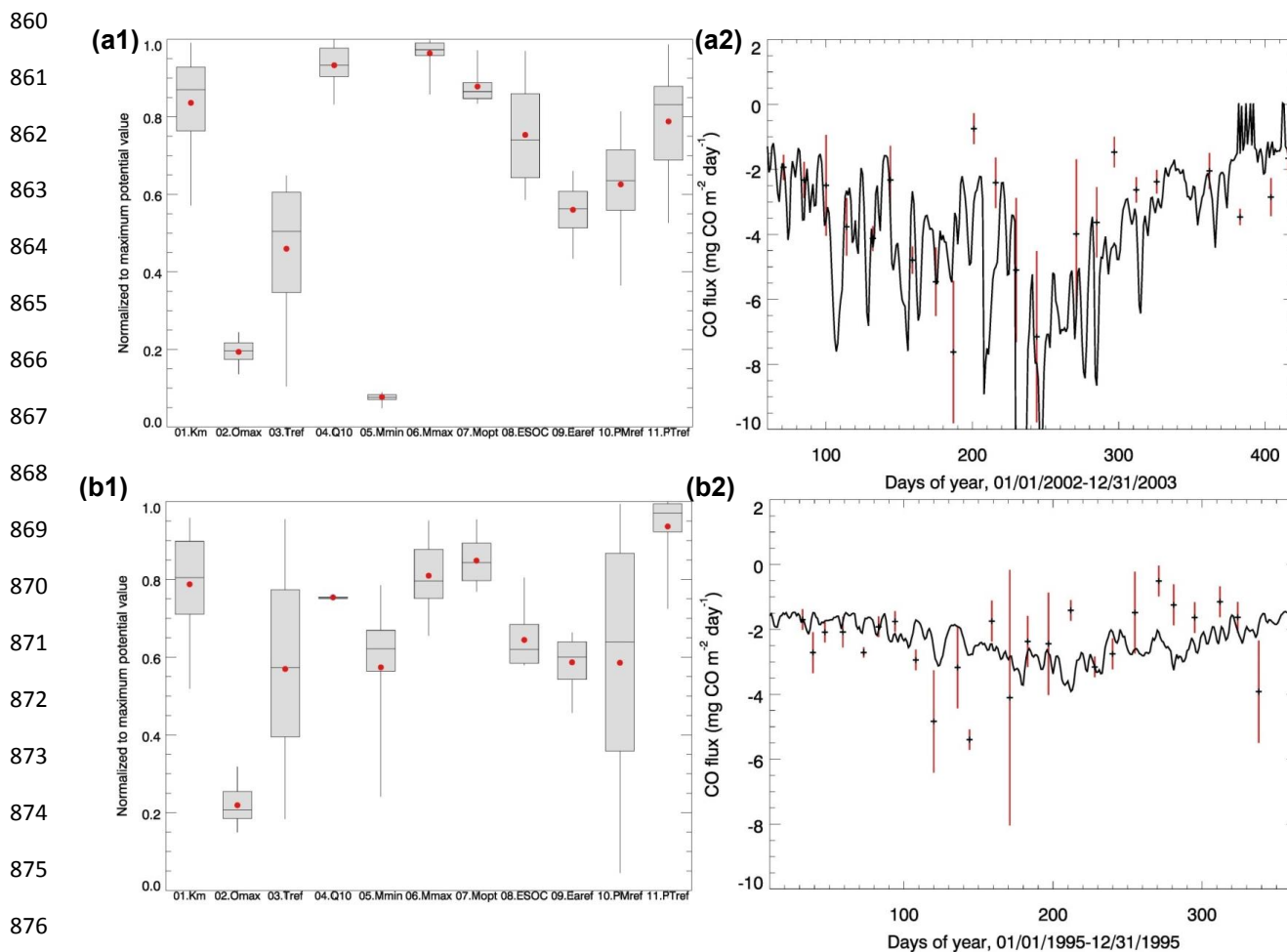
854

855

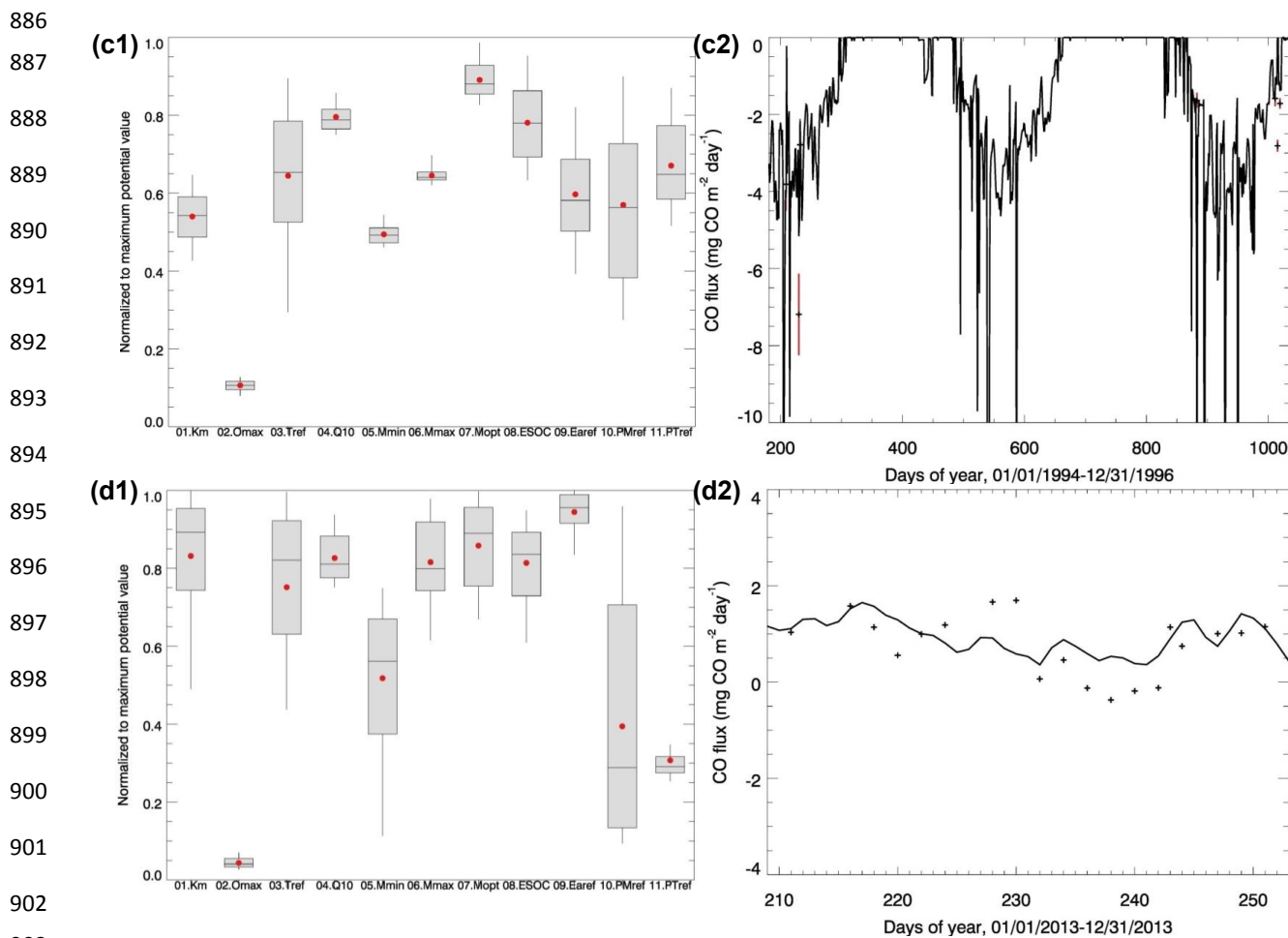


856

857 **Figure 2. Contd.** Evaluation of thermal and hydrology module at four sites: (c) Tropical Moist Forest, (d) Tropical Forest-
858 Savanna. (1) shows the soil temperature comparison between model simulations (gray line) and observations (black line)
859 and (2) shows the soil moisture comparison between model simulations (gray line) and observations (black line)

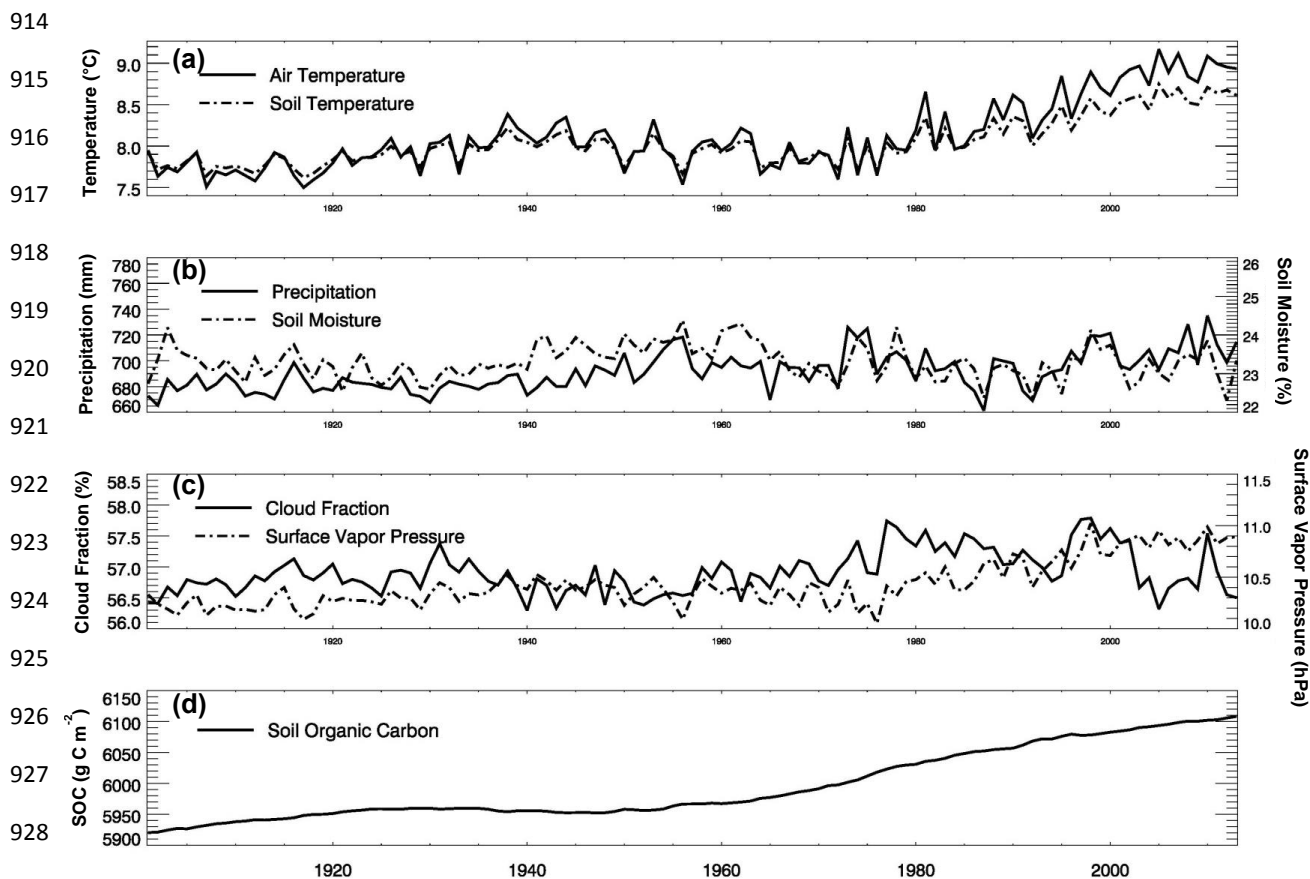


876
 877 **Figure 3.** Parameter ensemble experiment results: Each parameter has 50 calibrated values generated from running
 878 SCE-UA-R 50 times independently. Parameters are normalized to their largest potential values described in Table 2. (a1)
 879 and (a2) are temperate coniferous forest normalized parameter distribution boxplots and CO flux comparisons between
 880 model simulations (solid line, using mean value of parameters) and observations (“+”, red lines represent error bar),
 881 respectively. For each box, line top, box top, horizontal line inside box, box bottom and line bottom represent maximum,
 882 third quartile, median, first quartile and minimum of 50 parameter values. Red dot represents the mean value of 50
 883 parameter values. (b1) and (b2) are plots for temperate deciduous forest; (c1) and (c2) are for boreal forest; (d1) and (d2)
 884 are for grassland. Grassland observation data is the sum of hourly observations so there is no error bar presented.
 885



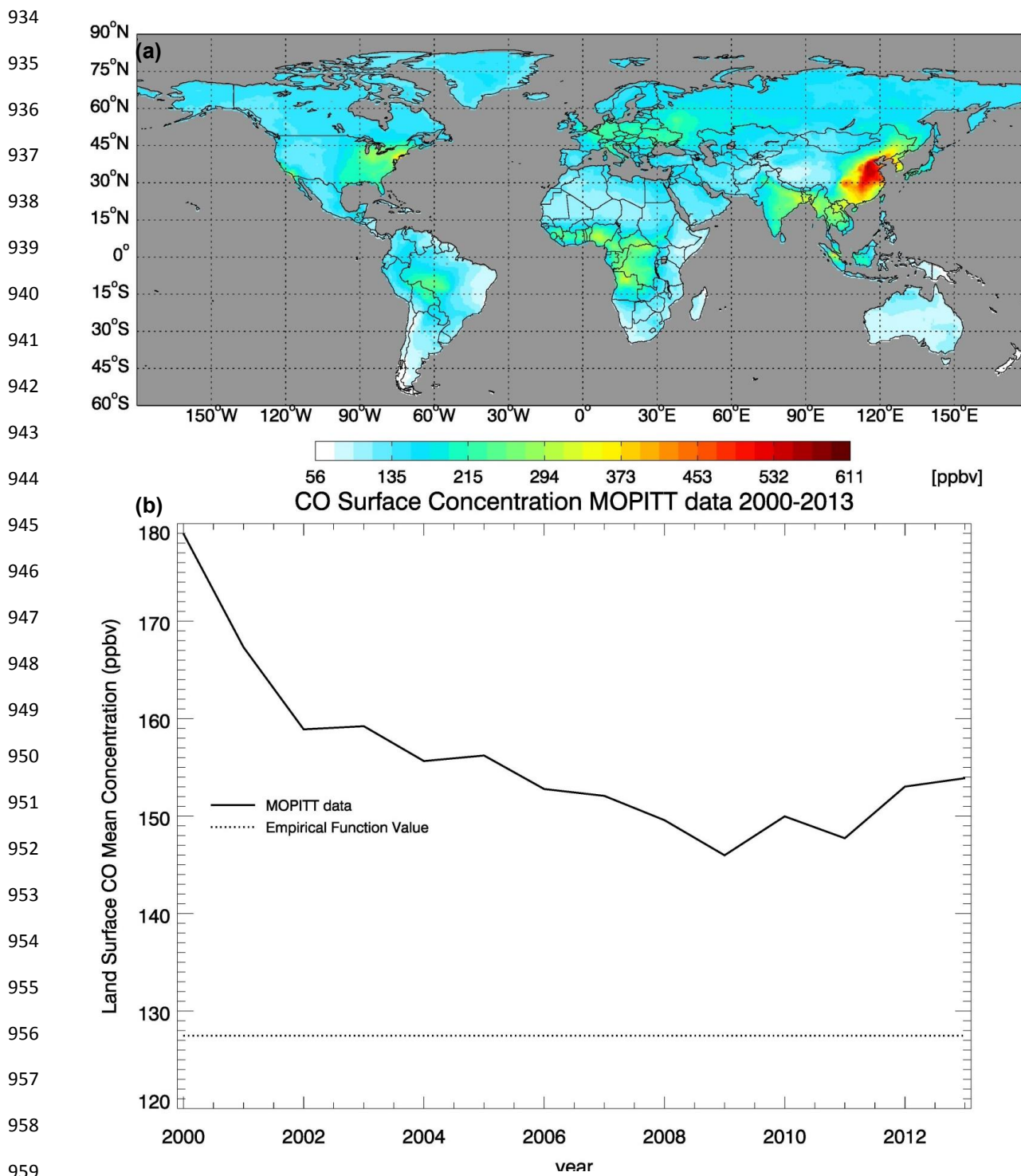
904 **Figure 3. Contd.** Parameter ensemble experiment results: Each parameter has 50 calibrated values generated from
905 running SCE-UA-R 50 times independently. Parameters are normalized to their largest potential values described in Table
906 2. (a1) and (a2) are temperate coniferous forest normalized parameter distribution boxplots and CO flux comparisons
907 between model simulations (solid line, using mean value of parameters) and observations (“+”, red lines represent error
908 bar), respectively. For each box, line top, box top, horizontal line inside box, box bottom and line bottom represent
909 maximum, third quartile, median, first quartile and minimum of 50 parameter values. Red dot represents the mean value
910 of 50 parameter values. (b1) and (b2) are plots for temperate deciduous forest; (c1) and (c2) are for boreal forest; (d1)
911 and (d2) are for grassland. Grassland observation data is the sum of hourly observations so there is no error bar
912 presented.

913

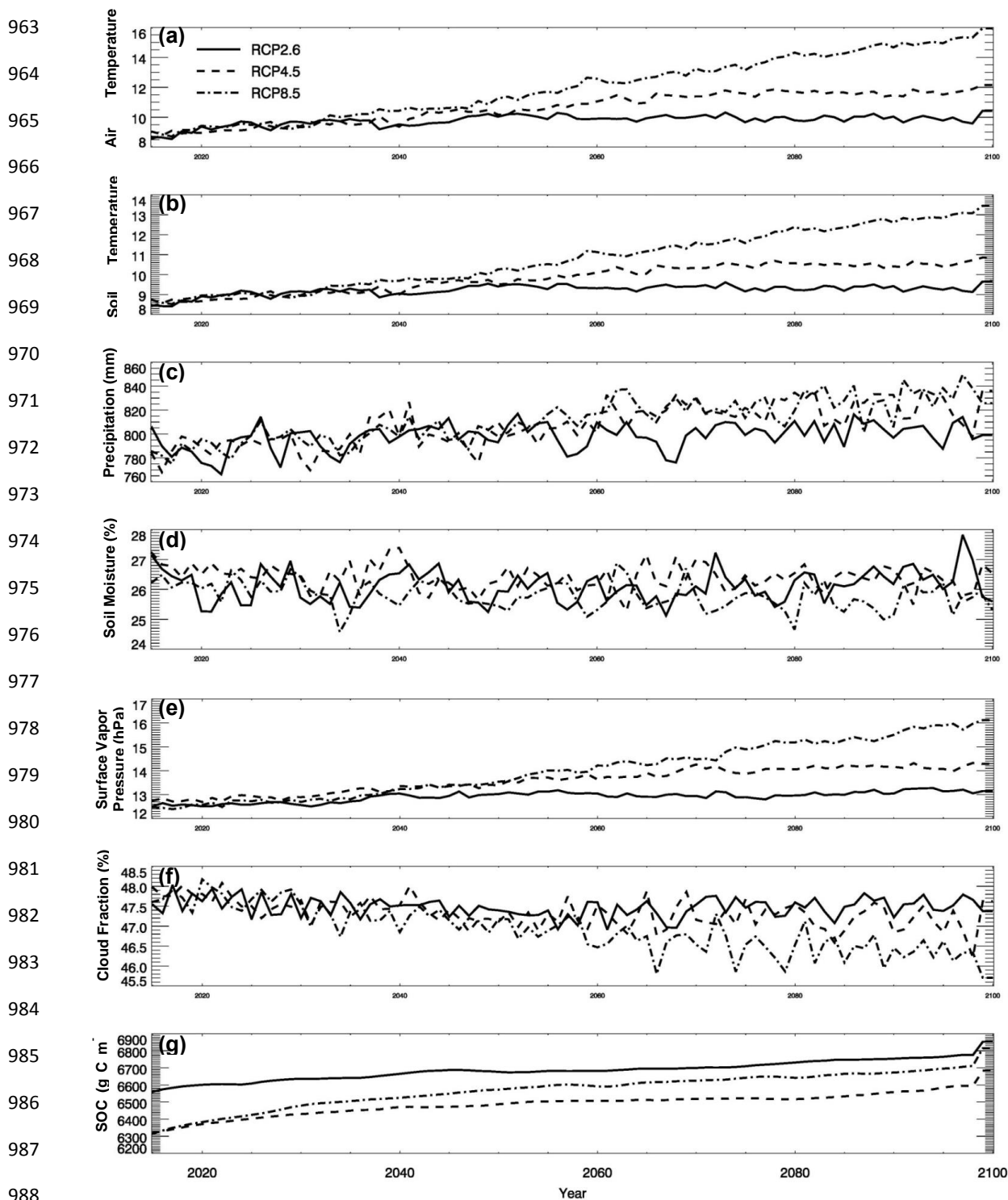


929
930 **Figure 4.** Historical global land surface mean climate, and simulated global mean soil moisture, soil temperature and
931 SOC for the period 1901-2013.
932

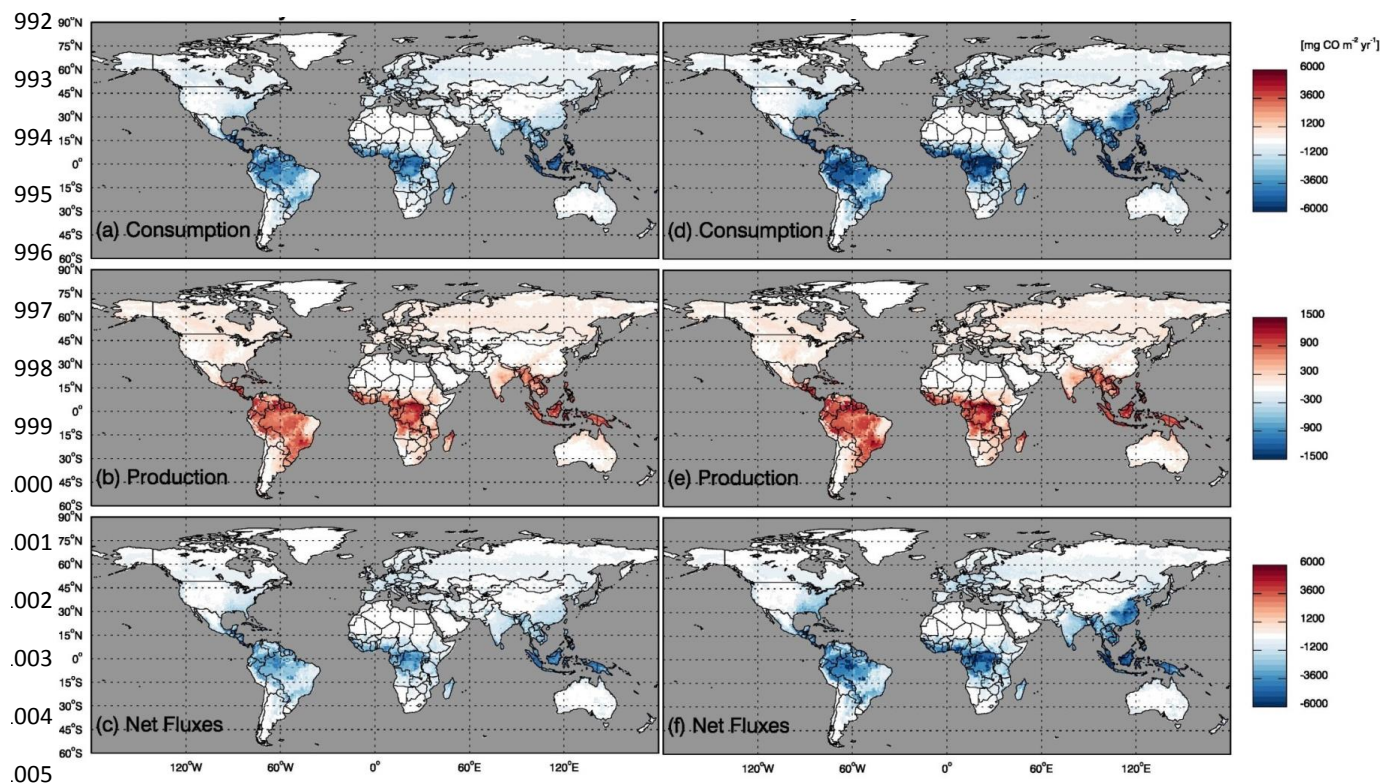
933



960 **Figure 5.** CO surface concentration data from MOPITT satellite (ppbv): (a) global mean CO surface concentrations from
961 MOPITT during 2000-2013; (b) the CO annual surface concentrations from both MOPITT and empirical functions (Potter
962 et al., 1996).



989 **Figure 6.** Global mean climate from RCP2.6, RCP4.5 and RCP8.5 data sets and simulated global mean soil temperature,
990 moisture and SOC: (a)-(g) are land surface air temperature (°C), soil temperature (°C), precipitation (mm), soil moisture
991 (%), surface water vapor pressure (hpa), cloud fraction (%), and SOC (mg m⁻²), respectively.



.006 **Figure 7.** Global annual mean soil CO fluxes ($\text{mg CO m}^{-2} \text{ yr}^{-1}$) during 1901-2013, estimated using constant CO
.007 concentration data (left side) and mean annual global soil CO fluxes during 2000-2013 using MOPITT CO atmospheric
.008 surface concentration data (right side)

.009

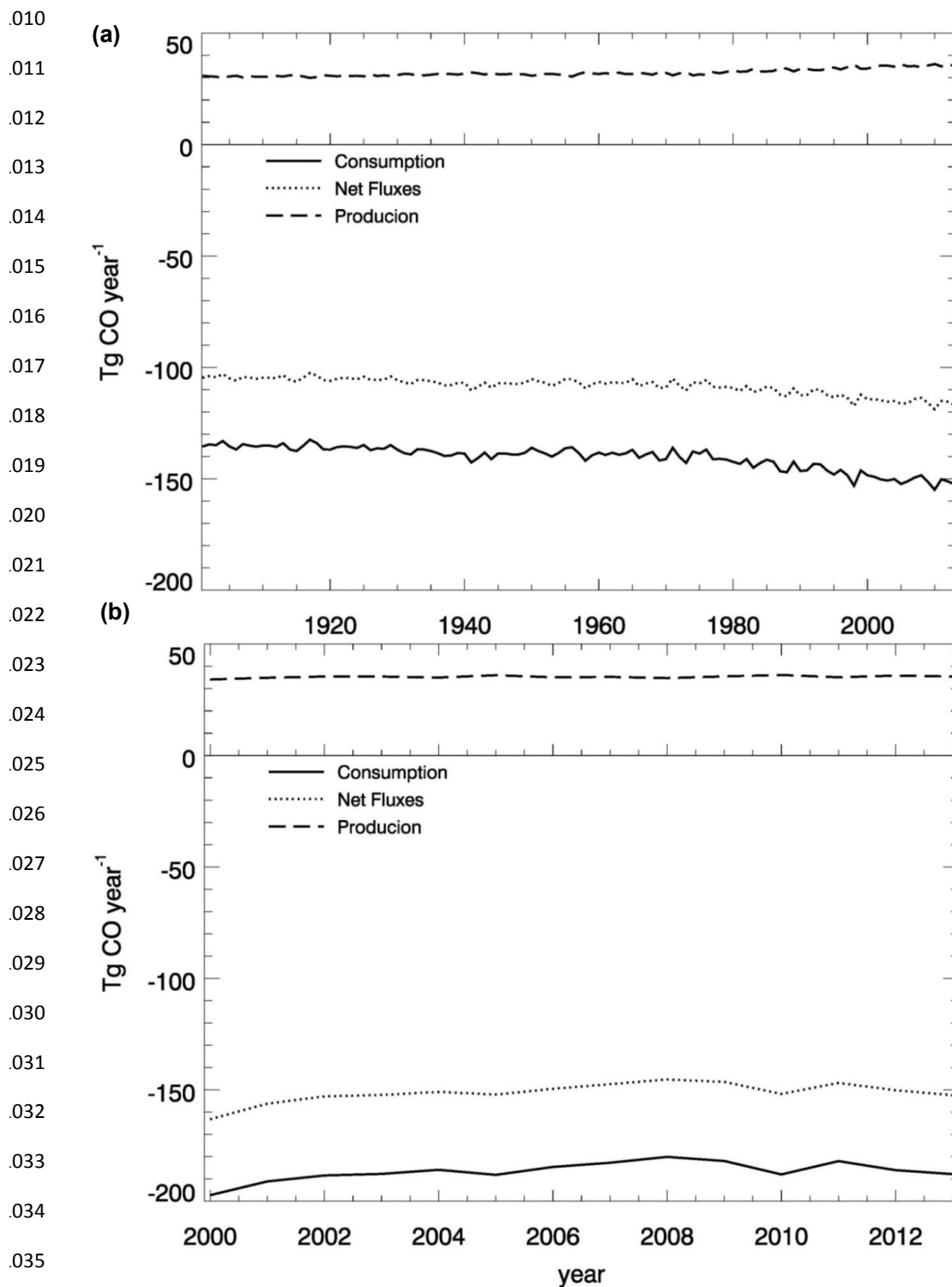


Figure 8. Global mean CO consumption, production and net flux (Tg CO yr⁻¹): (a) from 1901 to 2013, estimated with constant CO surface concentration data and (b) from 2000 to 2013 with MOPITT CO surface concentration data.

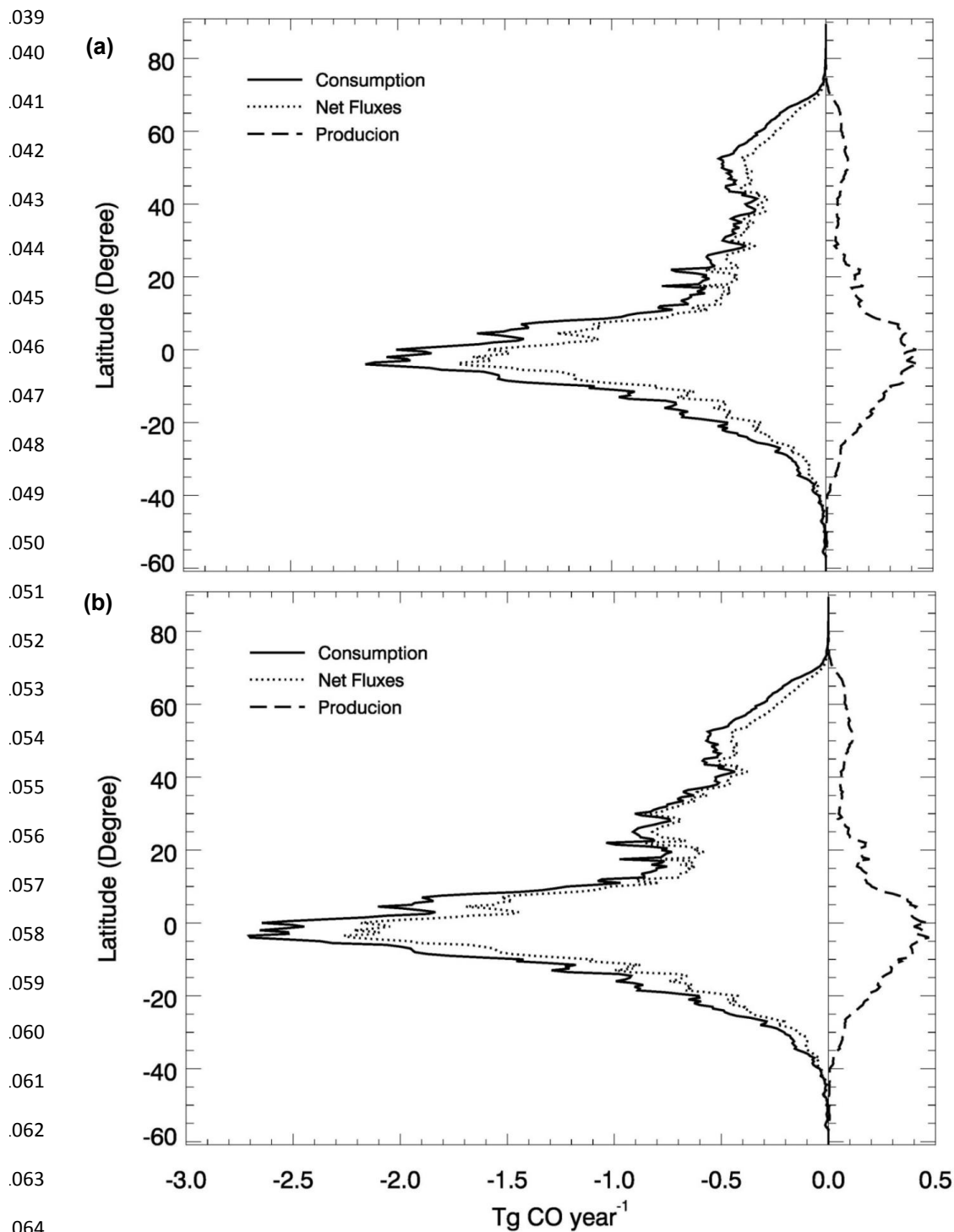


Figure 9. Global annual mean latitudinal distributions of soil CO consumption, production and net flux: (a) during 1901-2013 (Tg CO yr^{-1}) estimated with constant CO surface concentration data and (b) during 2000-2013 estimated with MOPITT CO surface concentration data.

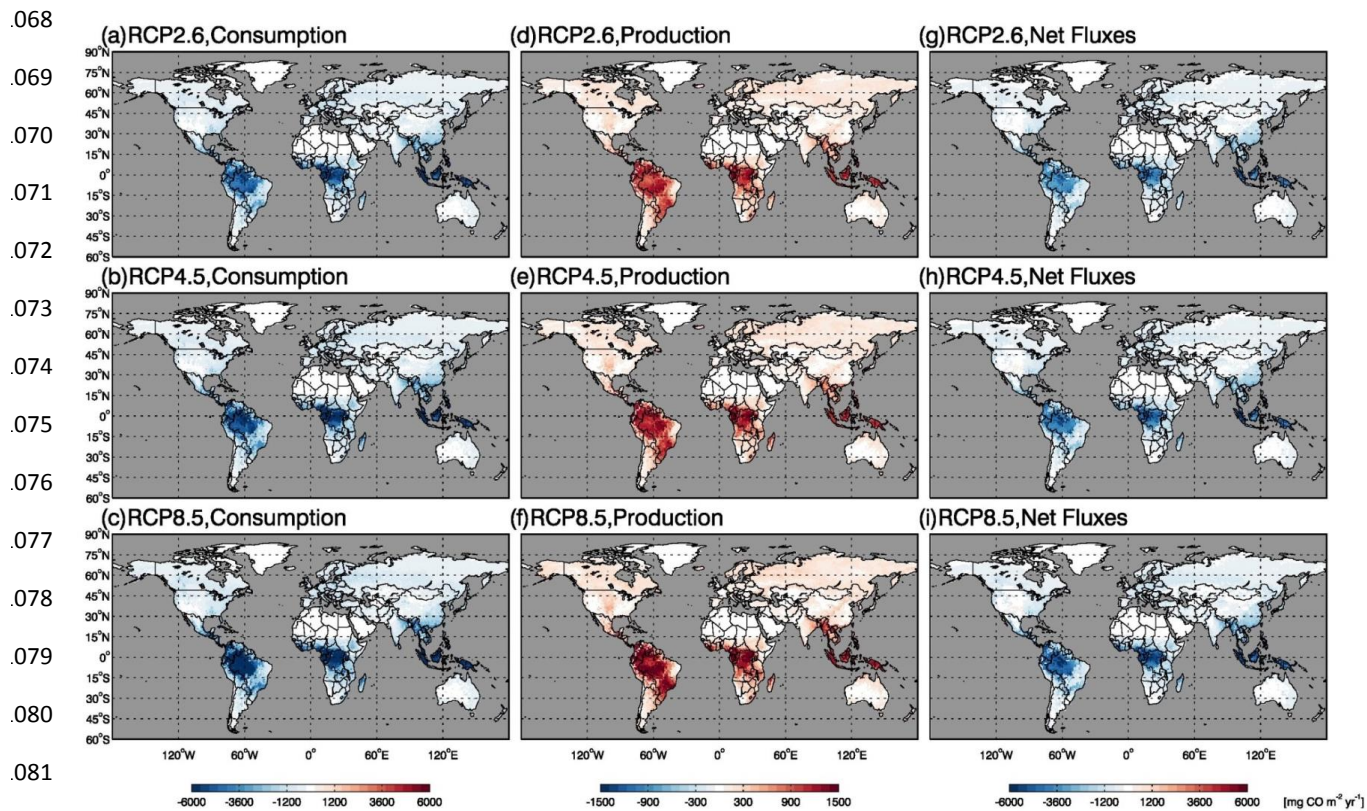
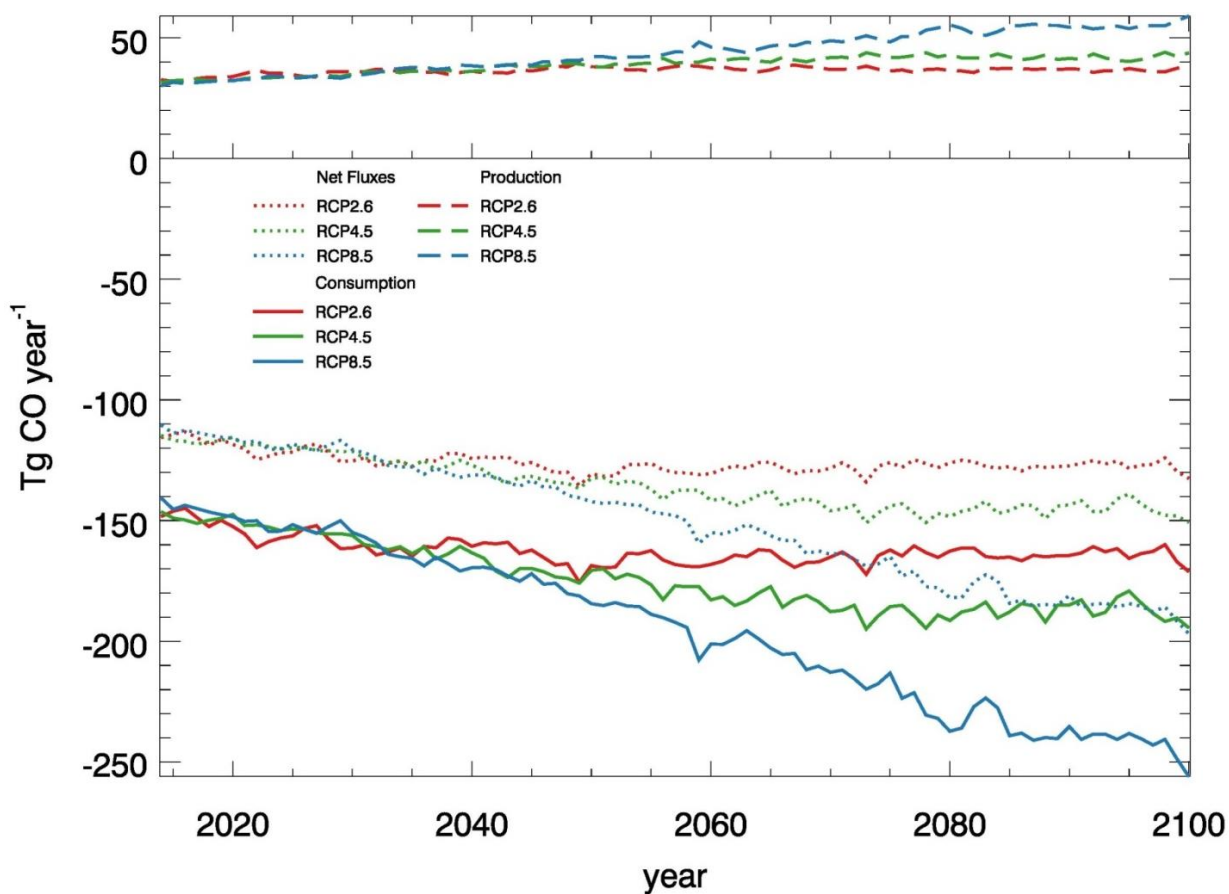


Figure 10. Global annual mean CO consumption, production and net flux (mg CO m⁻² yr⁻¹) under future climate scenarios RCP2.6, RCP4.5 and RCP8.5 during 2014-2100

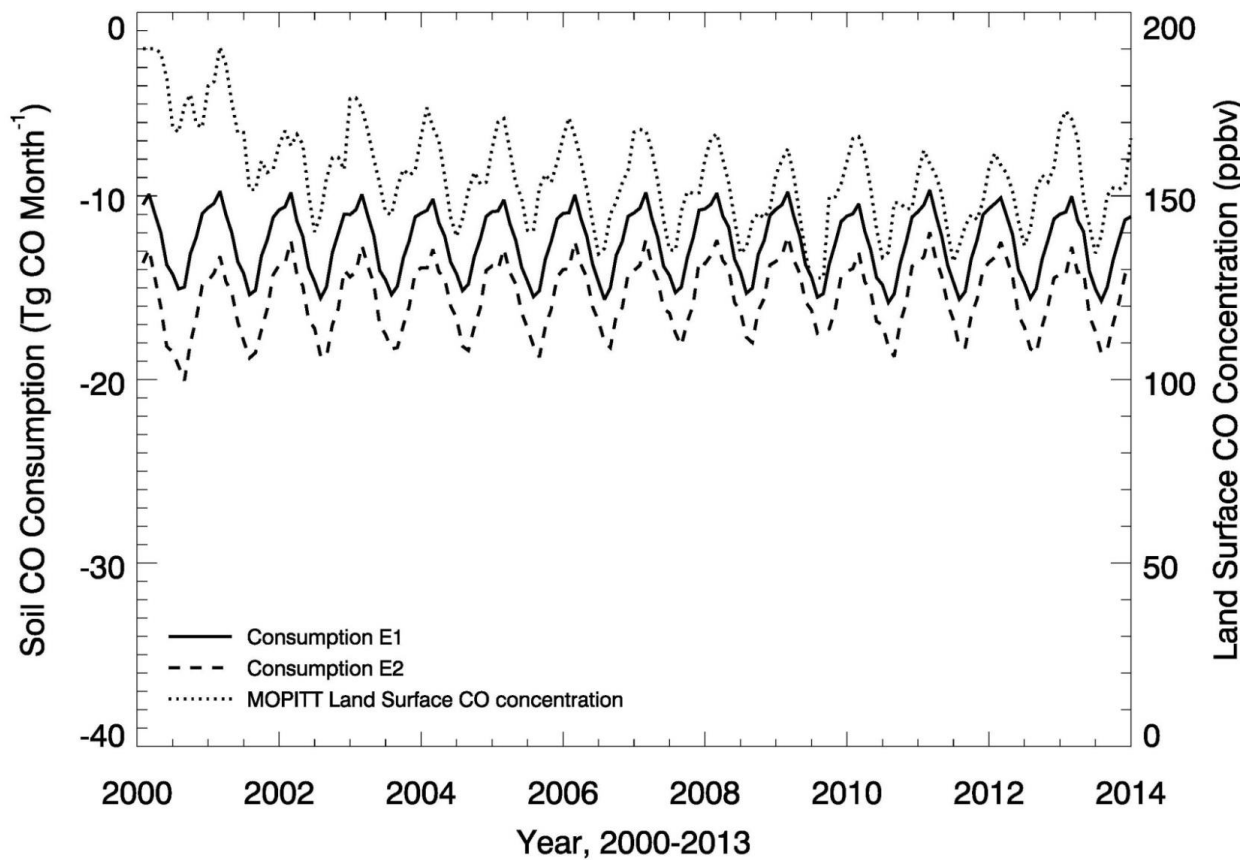
.084



.085

.086 **Figure 11.** Future Global mean soil CO consumption, net flux and production (Tg CO yr⁻¹) under future climate scenarios

.087 RCP2.6, RCP4.5 and RCP8.5 during 2014-2100



.088

.089 **Figure 12.** Monthly time series of MOPITT atmospheric CO concentration (ppbv) and soil CO consumption from model
.090 simulations E1 and E2 (Tg CO mon^{-1})